

On joint analysing *XMM-NuSTAR* spectra of active galactic nuclei

JIA-LAI KANG^{1,2} AND JUN-XIAN WANG^{1,2}

¹*CAS Key Laboratory for Research in Galaxies and Cosmology, Department of Astronomy, University of Science and Technology of China, Hefei, Anhui 230026, China; ericofk@mail.ustc.edu.cn, jxw@ustc.edu.cn*

²*School of Astronomy and Space Science, University of Science and Technology of China, Hefei 230026, China*

ABSTRACT

A recently released *XMM-Newton* technical note has revealed a significant calibration issue between *NuSTAR* and *XMM-Newton* EPIC, and provided an empirical correction to EPIC effective area. To quantify the bias caused by the calibration issue to joint analysis of *XMM-NuSTAR* spectra and verify the effectiveness of the correction, in this work we perform joint-fitting of *NuSTAR* and EPIC-pn spectra for a large sample of 104 observation pairs of 44 X-ray bright AGN. The spectra were extracted after requiring perfect simultaneity between *XMM-Newton* and *NuSTAR* exposures (merging GTIs from two missions) to avoid bias due to rapid spectral variability of AGN. Before the correction, the EPIC-pn spectra are systematically harder than corresponding *NuSTAR* spectra by $\Delta\Gamma \sim 0.1$, subsequently yielding significantly underestimated cutoff energy E_{cut} and the strength of reflection component R when performing joint-fitting. We confirm the correction is highly effective and can commendably erase the discrepancy in best-fit Γ , E_{cut} and R , and thus we urge the community to apply the correction when joint-fitting *XMM-NuSTAR* spectra. Besides, we show that as merging GTIs from two missions would cause severe loss of *NuSTAR* net exposure time, in many cases joint-fitting yields no advantage compared with utilizing *NuSTAR* data alone. We finally present a technical note on filtering periods of high background flares for *XMM-Newton* EPIC-pn exposures in the Small Window mode.

Keywords: Galaxies: active – Galaxies: nuclei – X-rays: galaxies

1. INTRODUCTION

The Nuclear Spectroscopic Telescope Array (*NuSTAR*; Harrison et al. 2013), the first direct-imaging hard X-ray mission with a spectral coverage from 3 to 79 keV, has remarkably boosted the study of various high-energy phenomenons. Active galactic nuclei are the dominant population in the extragalactic X-ray sky. According to the widely accepted disk-corona paradigm, the primary X-ray emission of AGN originates in a hot and compact region, namely the corona (Haardt & Maraschi 1991, 1993). The seed photons from the accretion disk are up-scattered to the X-ray band through inverse Comptonization, producing the observed power-law continuum, with a cutoff in the high energy end, which is a direct indicator of the coronal temperature T_e . For AGN studies, *NuSTAR* opens a new window to detect/measure the X-ray high energy cutoff E_{cut} (and

effectively, the corona temperature T_e) in many sources (e.g., Brenneman et al. 2014; Matt et al. 2015; Fabian et al. 2015; Kamraj et al. 2018; Baloković et al. 2020; Kang & Wang 2022). Meanwhile, *NuSTAR* observations are also essentially helpful to constrain the reflection component in the X-ray spectra (e.g., Parker et al. 2014; Kara et al. 2015; Wilkins & Gallo 2015; Panagiotou & Walter 2019).

In practice, *NuSTAR* data are often analysed in association with coordinated data of other X-ray missions, to achieve a broader energy coverage and higher spectral signal to noise ratio at < 10 keV, which could supposedly improve the constraints to X-ray spectral parameters. Among the coordinated missions, *XMM-Newton* (Jansen et al. 2001) is of most significance, with the longest coordinated observing time since *NuSTAR* Cycle 2¹. Thanks to the large effective areas of the EPIC

Corresponding author: Jia-Lai Kang & Jun-Xian Wang
 ericofk@mail.ustc.edu.cn, jxw@ustc.edu.cn

¹ https://heasarc.gsfc.nasa.gov/docs/nustar/nustar_prop.html

cameras, *XMM-Newton* could provide high-quality spectra in $0.3 - 10$ keV, as a nice complement to *NuSTAR*.

However, proper inter-instrument calibration is critical prior to analyzing joint observations from different observatories. A possible calibration issue between *NuSTAR* and *XMM-Newton* had been reported in literature (e.g., Cappi et al. 2016; Ponti et al. 2018; Middei et al. 2019). Such calibration issues could be the fundamental cause of the discrepancy in the measurements of E_{cut} or T_e in individual AGN, between studies fitting *NuSTAR* spectra alone (e.g., Kamraj et al. 2018; Rani et al. 2019; Kang et al. 2020; Panagiotou & Walter 2020; Akyolas & Georgantopoulos 2021; Kang & Wang 2022; Pal & Stalin 2023), and those joint-fitting quasi-simultaneous data from other missions (e.g., Marinucci et al. 2014; Tortosa et al. 2018; Zhang et al. 2018; Molina et al. 2019; Baloković et al. 2020; Hinkle & Mushotzky 2021; Kamraj et al. 2022; Pal et al. 2022).

The calibration issue between *NuSTAR* and *XMM-Newton* was confirmed by a recently released *XMM-Newton* calibration technical note², in which the EPIC-pn spectra of the Crab Nebula were found to be systematically harder than those of *NuSTAR*, with $\Gamma^{\text{pn}} - \Gamma^{\text{NuSTAR}} \sim -0.1$. An empirical correction of the effective area is then implemented (after SAS 20.0) in the newest *XMM-Newton* calibration files (but not deployed by default in the pipeline), improving the cross-calibration with *NuSTAR*. Such a correction however has not been adopted by most joint-analyses of *XMM-NuSTAR* spectra of AGN in literature. It is both technically and scientifically important to investigate how this calibration issue biases the X-ray spectral measurements of AGN, verify the effectiveness of the correction, and if yes, provide the updated X-ray spectral parameters after applying the calibration correction for AGN with joint *XMM-NuSTAR* observations.

2. SAMPLE AND DATA REDUCTION

We match the 817 Seyfert galaxies in the 105 month *Swift/BAT* catalog (Oh et al. 2018) with archival *NuSTAR* and *XMM-Newton* observations (as of 2023 August). In this work we focus on the EPIC-pn data of *XMM-Newton* (Strüder et al. 2001), which are most widely used in literature. However, the empirical correction of the effective areas for *XMM-Newton* EPIC-MOS (Turner et al. 2001) is exactly the same (see the calibration note in footnote 2), so the conclusions about the cross-calibration should also apply to the MOS data. We search for simultaneous observation pairs of the two

missions, requiring an overlapping exposure time > 5 ks between *NuSTAR* and EPIC-pn, obtaining 176 observation pairs of 94 sources. Note one *NuSTAR* exposure may overlap in time with more than one *XMM-Newton* exposures, and vice versa. Observation pairs with too few counts, or complicated spectra badly fitted with the model in Kang & Wang (2022), are further dropped, resulting in a final sample of 104 observation pairs (consisting of 100 *NuSTAR* and 102 *XMM-Newton* observations) of 44 sources (see Table 1)³.

Raw *NuSTAR* data are reduced with *nupipeline*, part of the HEASoft package (version 6.32.1), with calibration files of version 20210824. We extract the *NuSTAR* spectra using *nuproducts*, adopting a circular source region with a radius of $60''$ for each source, and an annulus from $120''$ to $150''$ for background extraction. Raw *XMM-Newton* data are processed with the Science Analysis Software (SAS 20.0.0) and current calibration files (CCF 3.13). We extract the source spectra from a circular region, the radius of which is optimally determined by *eregionanalyse*, with background from nearby source-free regions (see Figure 1 for example). *epatplot* is employed to confirm the pile-up effect is negligible in all the observations. Two ancillary response files (ARF) are created for each observation, with/without applying the aforementioned empirical correction of the effective area, by setting the parameter *applyabsfluxcorr* of the task *arfgen*. Finally, all the spectra are rebinned to attain a minimum of 50 counts per bin using *grppha*.

In the above paragraph we describe a typical process of the data reduction, but omit an ambiguous step of reducing the *XMM-Newton* data, i.e., filtering periods suffering from flaring background. Solar protons could produce flaring EPIC background, which is highly unpredictable and affects a large fraction of *XMM-Newton* observation time (Read & Ponman 2003; Carter & Read 2007). As recommended by the user guide⁴, a viable method is to extract a rate curve (usually with a time bin ≤ 100 s) in the source-free regions, of only valid single events with energy between 10 keV and 12 keV (“PATTERN==0 && PI IN [10000:12000]” in the expression of *evselect*). A new Good Time Interval (GTI) file will then be generated, dropping the periods with count rate above certain threshold, a recommended value of which

³ 21 observation pairs in this work were also adopted in the aforementioned technical note, but only used to show the improvement of the statistics (reduction of χ^2), irrelevant to the derivation of the empirical correction of ARF. We confirm the inclusion of these observations in this work does not bias our analysis.

⁴ https://xmm-tools.cosmos.esa.int/external/xmm_user_support/documentation/sas_usg/USG/epicbkgfiltering.html

² <https://xmmweb.esac.esa.int/docs/documents/CAL-TN-0230-1-3.pdf>

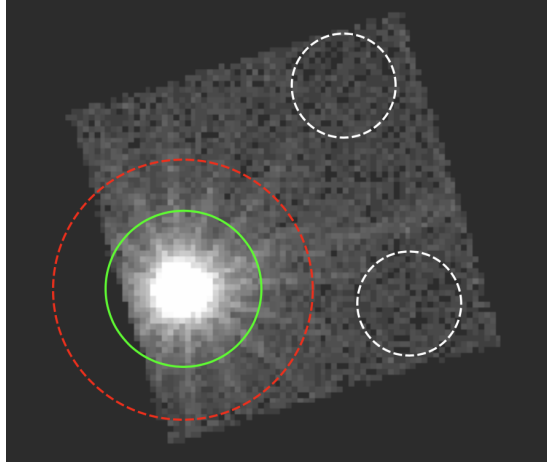


Figure 1. An example (*XMM-Newton* obsid 0741330101) of the adopted regions when processing the *XMM-Newton* EPIC-pn data in Small Window mode. The green circle is the source region, optimally determined by *eregionanalyse*, while the two white circles with a radius of $40''$ are the background regions. Outside the red circle with a radius of $100''$ is the source-free region, used to filter intervals with flaring background.

is 0.4 counts/s for the EPIC-pn camera in the Full Frame mode.

However, as shown in Table 1, most observations (85/102) of these bright AGN are operated in the Small Window mode (hereafter SW mode) to avoid serious pile-up effect, which has a much smaller FOV (1/36) than the Full Frame mode (hereafter FF mode). The value of the count rate threshold is hence supposed to be smaller for the SW mode, while the time bin of the rate curve should be large enough to contain sufficient counts. Therefore, for these SW observations, we try three different thresholds: 1) 0.4 counts/s, same as the FF mode; 2) 0.008 counts/s, scaled down because in the SW mode a much smaller sky area (see Figure 1) could be used to extract 10 – 12 keV light curve for high background filtering; and 3) 0.05 counts/s, a moderate threshold between 1) and 2); and adopt a time bin of 500 s. The consequent usable fraction of GTI is shown in Figure 2. Apparently, the threshold of 0.008 counts/s is too strict, leading to less than 40% GTI usable in more than half observations. Meanwhile, the threshold of 0.4 counts/s is likely too loose, causing insufficient filtering, the bias of which we shall show in §4.2. On the other hand, the threshold of 0.05 counts/s seems to be reasonable, and the corresponding distribution of usable GTI is similar to the one in Read & Ponman (2003), of a detailed study of EPIC background with FF observations.

Therefore, in our analyses below we adopt a threshold of 0.05 counts/s (unless otherwise stated, see the lower panel of Figure 3 for an example) to filter the flaring

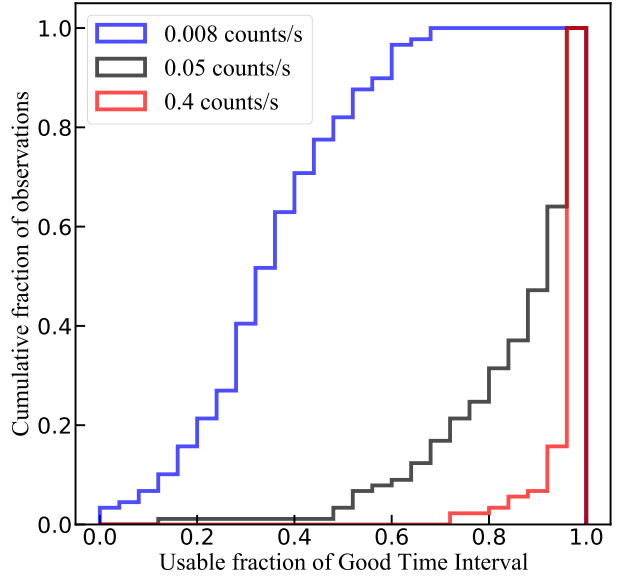


Figure 2. Usable fraction of the Good Time Interval after filtering the periods showing flaring background with different thresholds, for the 85 *XMM-Newton* exposures in SW mode.

background for SW observations⁵, while in §4.2, using *NuSTAR* spectra as reference, we shall show that such a threshold is indeed appropriate, whereas a looser threshold (0.4 counts/s) will lead to insufficient background subtraction and hence biased spectral parameters. After high background screening, the usable GTI of *NuSTAR* and EPIC-pn are merged to find the overlapped part (see Figure 3 for an example, and Table 2 for the net exposure time before/after the GTI merge for each *NuSTAR* exposure). The spectra of *NuSTAR* and EPIC-pn for a certain observation pair are then extracted from the overlapped GTI (i.e., with perfect simultaneity). This step is necessary to avoid potential bias caused by rapid X-ray spectral variability of AGN (e.g. Wu et al. 2020), that two spectra without perfect simultaneity may have intrinsically different spectral shape.

3. SPECTRAL FITTING

We perform spectral fitting using XSPEC (Arnaud 1996) and the χ^2 statistics. All the errors and the upper/lower limits of the parameters are derived following the $\Delta\chi^2 = 2.71$ criteria (corresponding to the 90% confidence level for one interesting parameter). Spectral fitting is carried out in the 3–78 keV band for *NuS-*

⁵ We adopt a threshold of 0.4 counts/s and 0.2 counts/s, for FF and LW observations respectively. The sample of them is too small to perform similar analysis.

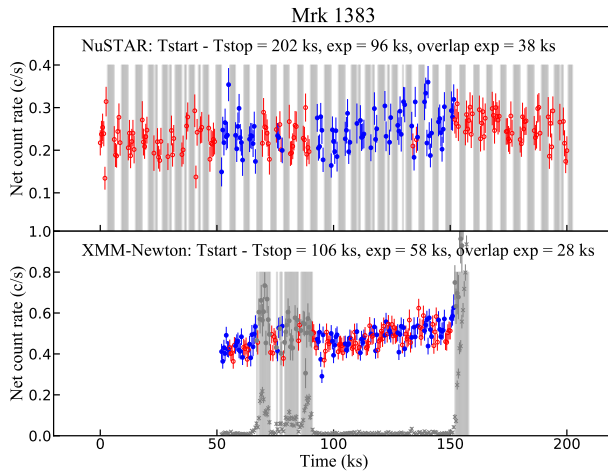


Figure 3. Example *NuSTAR* FPMA 3 – 78 keV (ObsID: 60501049002) and *XMM-Newton* EPIC-pn 3 – 10 keV (ObsID: 0852210101) light curves (with a time bin of 500 s) of Mrk 1383, to illustrate the merge of *NuSTAR* and EPIC-pn GTIs. The grey shades represent the dropped time intervals for each instrument, mainly due to the Earth occultation for *NuSTAR*, and flaring background for EPIC-pn. The blue dots represent the remaining data after merging the GTIs, while the red open circles mark the data dropped due to the merging of GTI. For EPIC-pn (lower panel), we over-plot the background rate curve (grey stars) used to filter the intervals with flaring background, and the corresponding data points filtered out from the source light curve (grey circles). The duration of the exposures and net exposure time (before/after merging GTIs) are labelled, respectively.

TAR and 3–10 keV band for EPIC-pn. We drop the data < 3 keV of EPIC-pn because 1) to avoid the influence of other spectral components, such as soft X-ray excess and complicated absorption features, in the soft band, and 2) the aforementioned empirical ARF correction for EPIC-pn is only available between 3 – 12 keV. For each *NuSTAR* observation, the spectra of FPMA and FPMB are jointly fitted with a cross-normalization (Madsen et al. 2015).

Following Kang & Wang (2022), we employ the model *zphabs* \times (*pexrav* + *zgauss*) to fit the spectra. Among them, *zphabs* models the intrinsic photoelectric absorption, *pexrav* (Magdziarz & Zdziarski 1995) models an exponentially cut-off power law with a neutral reflection component, and *zgauss* models the Fe K α line. During the fitting, the absorption column density N_{H} , photon index Γ , high energy cutoff E_{cut} , reflection strength R are set free to vary. We deal with the Fe K α line in the same way as Kang & Wang (2022). We firstly fix the line at 6.4 keV in the rest frame and the line width at 19 eV (the mean Fe K α line width in AGNs measured with

Chandra HETG; Shu et al. 2010) to model a neutral narrow Fe K α line. Then we set the line width free to vary and adopt the corresponding results if such a variable line width prominently improves the fitting ($\Delta\chi^2 > 5$). To simultaneously show the discrepancy between two missions and how the measurement of E_{cut} and R is biased, we conduct both independent and joint fit of the *NuSTAR* and EPIC-pn spectra. We firstly fit the *NuSTAR* spectra alone and obtain the best-fit parameters (Γ^{Nu} , $E_{\text{cut}}^{\text{Nu}}$ and R^{Nu} in Table 1). Then we fit the corresponding EPIC-pn spectrum, with E_{cut} and R fixed at the best-fit results of *NuSTAR* spectra, as both parameters are barely constrained by EPIC-pn data. We then derive Γ^{pn} and $\Gamma^{\text{pn}-\text{Cor}}$, for effective area uncorrected/corrected EPIC-pn data respectively, to highlight the effect of the calibration issue and the correction. Finally, we jointly fit the *NuSTAR* and EPIC-pn spectra to measure the $E_{\text{cut}}^{\text{joint}}$, R^{joint} , $E_{\text{cut}}^{\text{joint}-\text{Cor}}$, and $R^{\text{joint}-\text{Cor}}$. During the joint-fitting, all the parameters of the EPIC-pn spectrum are linked with *NuSTAR* spectra, except a variable constant to account for the absolute normalization between the two missions.

4. DISCUSSION

4.1. The calibration between *NuSTAR* and *XMM-Newton*

We show the best-fit Γ of *NuSTAR* and EPIC-pn spectra in Figure 4. Patently, the EPIC-pn spectra without the correction are systematically and significantly harder than the coordinated *NuSTAR* spectra. Specifically, we find that mean $\Gamma^{\text{Nu}} = 1.84 \pm 0.02$, while mean $\Gamma^{\text{pn}} = 1.74 \pm 0.02$. Meanwhile, the empirical correction of the effective area seems able to completely erase the discrepancy, resulting in mean $\Gamma^{\text{pn}-\text{Cor}} = 1.84 \pm 0.02$. Furthermore, the two subsamples of observations before/after 2017-01-01 (roughly equally divided) show that the discrepancy does not evolve with time.

In Figure 5 we compare the joint-fitting derived E_{cut} and R (before and after applying the correction respectively) with those derived through fitting *NuSTAR* spectra alone. Apparently, the smaller Γ^{pn} also leads to smaller E_{cut} and R when perform joint-fitting, due to the strong positive degeneracy between Γ and E_{cut} as well as between Γ and R (e.g., Molina et al. 2019; Panagiotou & Walter 2020; Kang et al. 2021; Kang & Wang 2023). Meanwhile, the correction is also highly effective for these two parameters.

Therefore, without the correction, the calibration issue between *NuSTAR* and EPIC-pn will bias the measured E_{cut} and R towards lower values. We note the exact strength of the bias would depend on the statistical significance of the EPIC-pn data. Note in this work

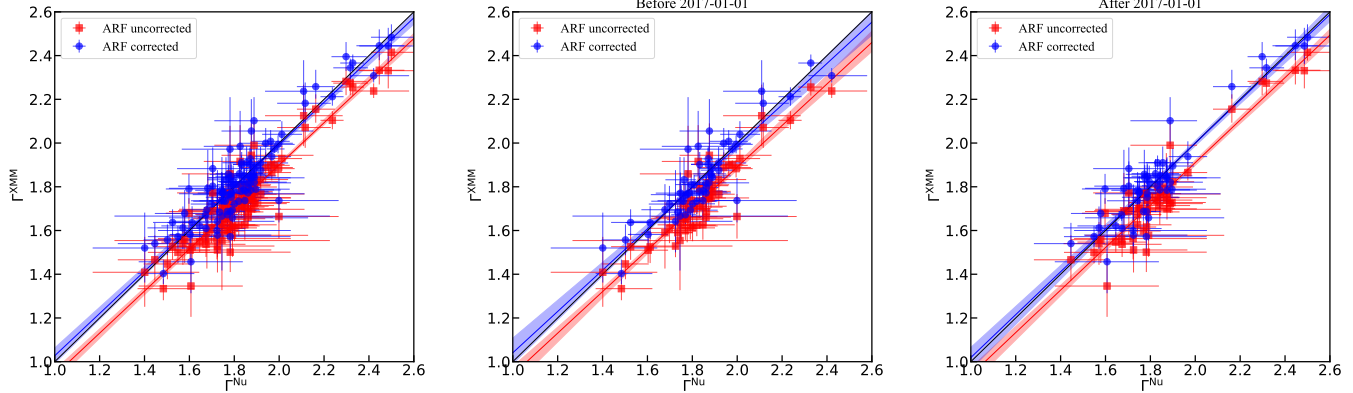


Figure 4. The left panel: photon index Γ of the *NuSTAR* spectra versus those of the EPIC-pn spectra before (red square) or after (blue circle) correcting the effective area (corresponding to Γ^{Nu} , Γ^{pn} and $\Gamma^{\text{pn-Cor}}$ in Table 1 respectively). The colored solid lines show the linear regression results (in comparison with the black 1:1 line), with the shadows showing the 1σ uncertainty derived through bootstrapping the sample. The middle and right panels show the case for observations before/after 2017-01-01.

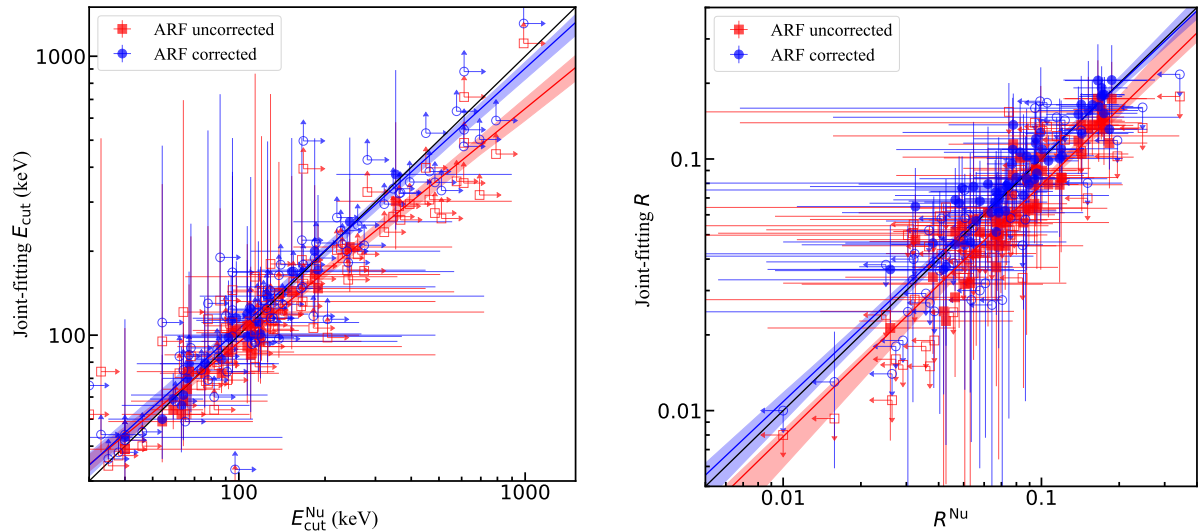


Figure 5. E_{cut} and R derived through fitting the *NuSTAR* spectra alone versus joint-fitting with EPIC-pn spectra. We perform linear regression in logarithmic space with *asurv* (Feigelson & Nelson 1985) to handle the censored data points (as hollow markers). The colored solid lines show the linear regression results (in comparison with the black 1:1 line), with the shadow showing the 1σ uncertainty derived through bootstrapping the sample.

we require a perfect simultaneity between *NuSTAR* and EPIC-pn data to avoid additional bias due to intrinsic spectral variation, which is not the case in most works. Neglecting the intrinsic variability, the effect of the bias would be stronger if the EPIC-pn exposure is longer than the *NuSTAR* one, as relatively longer EPIC-pn exposure could enhance the dominance of the uncorrected EPIC-pn spectrum's contribution to the joint fitting. Besides, for sources at high redshift or with high accretion rate and very steep spectra (e.g., Lanzuisi et al. 2016, 2019;

Tortosa et al. 2021), the bias is also expected to be more serious as the EPIC-pn data could be more dominant during the spectral fitting in these cases. We therefore urge the community to adopt the *XMM-Newton* ARF correction when joint-fitting *XMM-NuSTAR* spectra spectra (but note the correction at < 3 keV is yet unavailable).

Moreover, although in this work we focus on how the measurements of Γ , E_{cut} and R are biased, the calibration issue could also bias the measurements of other

parameters derived through joint fitting, for example, the spin of the blackhole a (e.g., Risaliti et al. 2013; Porquet et al. 2019; Jiang et al. 2022) and the absorption column density N_{H} in Compton-thick sources (e.g., Marchesi et al. 2022; Silver et al. 2022; Sengupta et al. 2023). Compared with E_{cut} and R , deriving these parameters is more model-dependent and the effect of the bias should be inspected case by case (which is beyond the scope of this work).

4.2. Filter the flaring background of *XMM-Newton* in Small Window mode

Using *NuSTAR* spectra as references for ARF corrected *XMM-Newton* EPIC-pn spectra, we investigate how the choice of the threshold count rate to filter high background flares affects the spectral fitting results. For the *XMM-Newton* SW mode observations, we now take a threshold of 0.4 counts/s to filter high background intervals, regenerate the common GTI, and in which we extract the corresponding *NuSTAR* and EPIC-pn spectra. To highlight the impact of the flaring background, we limit the comparison to the observations with significant background flaring, through requiring that in $> 10\%$ of all usable GTI, the 10 – 12 keV count rate of the light curve we generated to filter background flares lies between 0.05 and 0.4 counts/s. 33 of the 89 SW observations pairs meet this criterion, the Γ^{Nu} versus $\Gamma^{\text{pn-Cor}}$ of which are shown in Figure 6.

After applying the *XMM-Newton* released ARF correction, the *XMM-Newton* EPIC-pn spectra generated with a filtering threshold of 0.4 counts/s are still slightly harder than the *NuSTAR* ones (see Figure 6), indicating the fitting is biased. We interpret the bias as an underestimation of the flaring (soft protons induced) background, as their spectra are apparently much harder than those of AGN (see §4 in Kuntz & Snowden 2008), the underestimation of which will hence lead to a harder net spectrum. For SW observations, the target object is always placed near the aim point of the telescope, where the flaring background will be stronger than that in the region used for background subtraction, due to the vignetting effect of the background flares (see Figure 17 in Kuntz & Snowden 2008). Our finding shows that despite the small FOV of the SW mode, the spatial unevenness of the background is non-negligible when the flaring background is strong and not properly filtered, which will bias the spectral fitting even for these bright AGN.

On the other hand, Figure 6 also confirms that a threshold of 0.05 counts/s is appropriate to filter high background flares in the Small Window mode of *XMM-Newton* EPIC-pn observations. After filtering back-

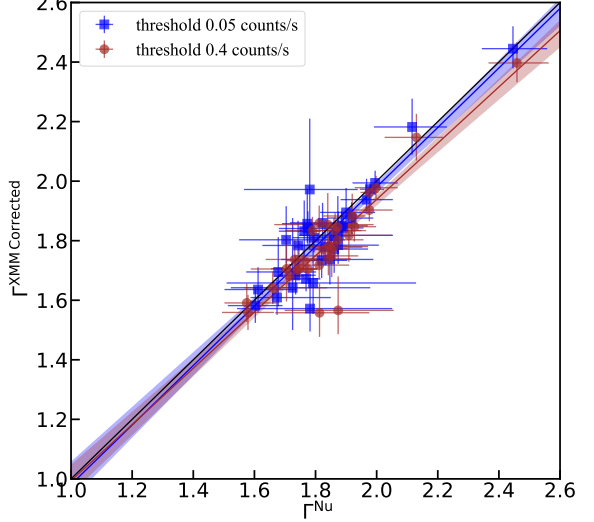


Figure 6. The photon index Γ (y-axis) derived using the effective area corrected *XMM-Newton* EPIC-pn spectra, after filtering the periods showing flaring background with a threshold of 0.05 counts/s (blue squares) or 0.4 counts/s (brown circles), versus those derived using *NuSTAR* spectra (x-axis), for the 33 observation pairs with significant flaring background. The colored solid lines show the linear regression results (in comparison with the black 1:1 line), with the shadow showing the 1σ uncertainty derived through bootstrapping the sample.

ground flares, the residual quiescent soft protons induced background, along with other potential components (e.g., De Luca & Molendi 2004), cause no significant bias at least for these bright AGN.

4.3. Do simultaneous *XMM-Newton* data really help?

As shown above, applying the *XMM-Newton* released ARF correction is highly effective, making the joint-fitting of *NuSTAR* and *XMM-Newton* spectra valid and feasible. However, compared with Kang & Wang (2022) which fits the *NuSTAR* spectra alone, it seems that the joint-fitting in this work does not significantly improve the constraints to the spectral parameters. Due to various observational restrictions, the proposed coordinated observations of *NuSTAR* and *XMM-Newton* often can not perfectly overlap (see Figure 3). Moreover, filtering the periods with flaring background for *XMM-Newton* also loses exposure time (see also Figure 3). Therefore, if one requires a perfect simultaneity between *NuSTAR* and *XMM-Newton* data as this work does, the involvement of *XMM-Newton* data leads to loss of *NuSTAR* exposure time and hence does not always improve the fitting. As shown in Table 2 and Figure 7, about 50% of the observations will lose more than 50% of the *NuSTAR* exposure time, if requiring a perfect simultaneity

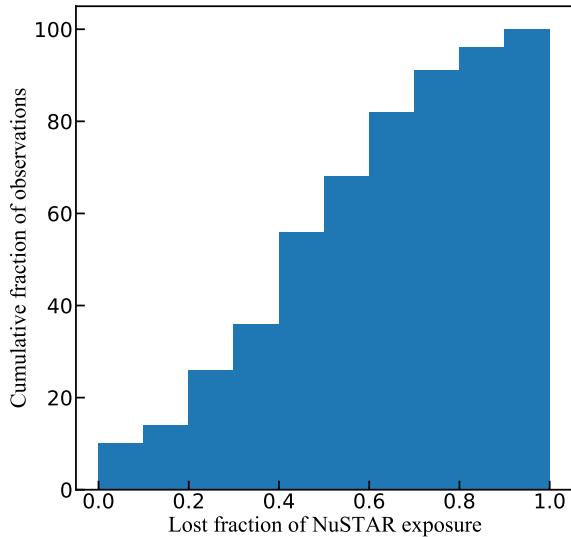


Figure 7. Lost fraction of the *NuSTAR* net exposure after requiring a perfect simultaneity between *NuSTAR* and *XMM-Newton* data.

between *NuSTAR* and *XMM-Newton* data. We illustrate an example of Mrk 1383 in Figure 3, of which a 100 ks coordinated *NuSTAR* and *XMM-Newton* observation was proposed. We first note that for a long *NuSTAR* observation in science mode, only about 50% of the duration time is available for exposure due to the Earth occultation. Therefore, a proposed 100 ks *NuSTAR* exposure is actually discontinuously distributed in a ~ 200 ks duration, indicating it can never be perfectly simultaneous with a 100 ks long *XMM-Newton* exposure. In the example we show in Figure 3 for Mrk 1383, the unique distribution of *NuSTAR* exposure directly causes a loss of $\sim 50\%$ net exposure time for both *NuSTAR* and *XMM-Newton* if requiring a perfect simultaneity. Furthermore, filtering the intervals with flaring background for *XMM-Newton* causes a further loss of the exposure time. Taken together, inclusion of the *XMM-Newton* data causes a loss of more than 60% of the *NuSTAR* net exposure time. Note for the Small Window mode of EPIC-pn, the livetime fraction is only 71%. This leads to a shorter net exposure time of *XMM-Newton* (28 ks) than *NuSTAR* one (38 ks) after merging the GTIs, which further reduces the statistical significance of *XMM-Newton* data.

To conduct a quantified assessment, we extract *NuSTAR* spectra in all the available GTI (without a match with EPIC-pn) and fit them with the same model, the result of which is shown in Table 2. In Figure 8, we show the distribution of the relative errors of Γ , R and E_{cut} , along with the detection fraction of R and E_{cut} . In con-

clusion, for this sample and this model, the involvement of *XMM-Newton* data does not significantly help.

If we make a concession about the simultaneity, simply including a quasi-simultaneous *XMM-Newton* exposure will certainly improve the constraint of the spectral parameters, which however could bring biases for variable sources like AGN. Moreover, here we adopt *pexrav*, a simple model without strong physical assumptions, to model the reflection component, while models like *pexmon* (Nandra et al. 2007), *xillver* and *relxill* (Dauser et al. 2010; García et al. 2014) perform self-consistently fitting on the reflection component and the Fe K α line. EPIC spectra will be statistically more significant on the constraint of E_{cut} and R when fitting with these models, as they provide good constraint for the Fe K α line. However, we stress the coupling between the reflection component and Fe K α line is yet unclear (Chiang et al. 2000; Mantovani et al. 2016; Kang et al. 2020). Finally, we note the current correction of the effective area is limited to 3–12 keV, indicating the EPIC data below 3 keV are not usable when performing joint-fitting with *NuSTAR*. With proper soft band correction and wider dynamic range, EPIC spectral would be statistically more important, though the complicated absorption and soft excess in the soft band might induce other biases.

5. SUMMARY

In this work we perform joint-fitting of *NuSTAR* and *XMM-Newton* EPIC-pn spectra for a large sample of 104 observation pairs of 44 AGN. Below are our main results.

- Calibration issue does exist between two missions; EPIC-pn spectra are systematically harder than those of *NuSTAR* ($\Delta\Gamma \sim 0.1$), leading to underestimated cutoff energy E_{cut} and reflection component R when performing joint-fitting before correcting the calibration issue.
- The empirical correction of the effective area implemented in latest *XMM-Newton* calibration files (but would not be applied by default) is highly effective and could commendably erase the discrepancy in the derived best-fit Γ , E_{cut} and R .
- For this sample, requiring a perfect simultaneity between the *NuSTAR* and EPIC-pn spectra leads to serious loss of net exposure time of *NuSTAR*. Consequently, fitting *NuSTAR* spectra jointly with simultaneous EPIC-pn data does not always improve the constraints to the key spectral parameters.

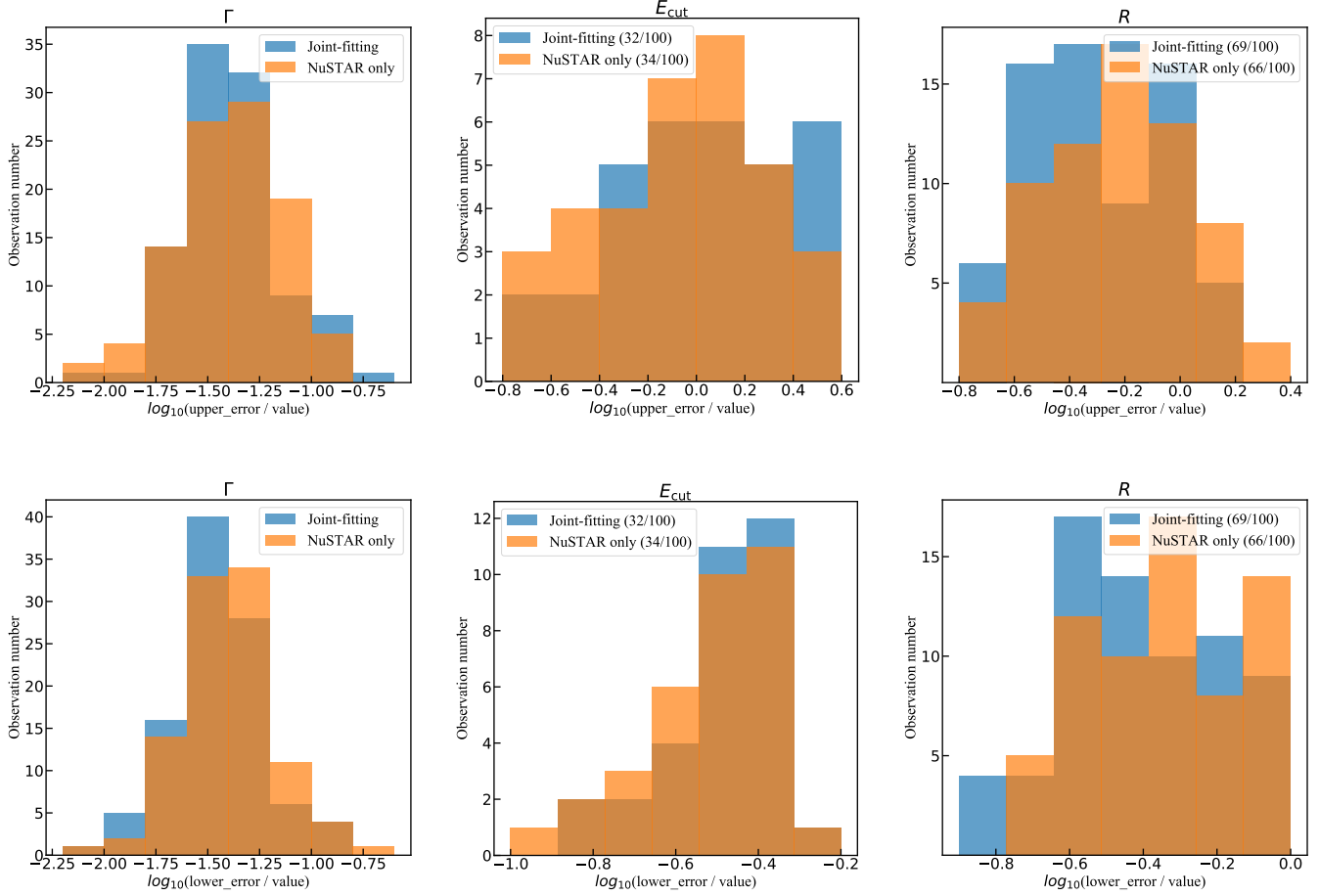


Figure 8. The distribution of the relative errors of Γ , R and E_{cut} , with the detection fraction of R and E_{cut} provided in the legend. Blue boxes show the results of the joint-fitting of *NuSTAR* and EPIC-pn, while the orange boxes show the result of fitting the *NuSTAR* spectra only (from the whole *NuSTAR* exposure without matching EPIC-pn GTI).

- For *XMM-Newton* EPIC-pn observations in Small Window mode, insufficient filtering of high background flares could bias the spectral fitting results due to the background vignetting effect, which is no longer negligible in case of background flares. A threshold of 0.05 counts/s to filter background flares (see §2 for the definition) appears appropriate for EPIC-pn Small Window mode.

Finally, we note again the correction of the effective area is not applied by default in *arfgen*. Currently, the correction is limited to 3–12 keV and thus not applicable if the soft X-ray band data are included. If a similar calibration issue exists below 3 keV, the twisted response curve itself could bias the measurement of the soft excess and ionized absorption, even when fitting the EPIC-pn spectrum alone. We look forward to an updated correction curve in future calibration releases.

ACKNOWLEDGMENTS

This research has made use of the *NuSTAR* Data Analysis Software (NuSTARDAS) jointly developed by the ASI Science Data Center (ASDC, Italy) and the California Institute of Technology (USA). This work is based on observations obtained with *XMM-Newton*, an ESA science mission with instruments and contributions directly funded by ESA Member States and NASA. This work is supported by National Natural Science Foundation of China (grants No. 11890693, 12033006 & 12192221). The authors gratefully acknowledge the support of Cyrus Chun Ying Tang Foundations.

Table 1. Fitting results of NuSTAR, XMM, and joint spectra (requiring perfect simultaneity between NuSTAR and XMM exposures)

Source	Nu ID	XMM ID	Mode	Γ^{Nu}	Γ^{pn}	$\Gamma^{\text{pn-Cor}}$	$E_{\text{cut}}^{\text{Nu}}$	$E_{\text{cut}}^{\text{joint}}$	$E_{\text{cut}}^{\text{joint-Cor}}$	R^{Nu}	R^{joint}	$R^{\text{joint-Cor}}$
				keV	keV	keV						
Fairall 9	60001130002	0741330101	SW	1.78 $^{+0.16}_{-0.21}$	1.86 $^{+0.22}_{-0.20}$	1.97 $^{+0.24}_{-0.20}$	> 38	> 37	> 38	< 1.05	< 1.34	< 1.67
Mrk 359	60402021004	0830550901	SW	1.84 $^{+0.14}_{-0.12}$	1.71 $^{+0.09}_{-0.09}$	1.79 $^{+0.09}_{-0.09}$	> 95	> 89	> 99	0.85 $^{+0.97}_{-0.58}$	0.56 $^{+0.72}_{-0.44}$	0.72 $^{+0.79}_{-0.46}$
	60402021006	0830551001	SW	1.84 $^{+0.04}_{-0.11}$	1.75 $^{+0.09}_{-0.09}$	1.82 $^{+0.09}_{-0.08}$	> 109	> 112	> 125	0.53 $^{+0.72}_{-0.43}$	0.32 $^{+0.56}_{-0.31}$	0.47 $^{+0.59}_{-0.35}$
	60402021008	0830551101	SW	1.78 $^{+0.27}_{-0.24}$	1.50 $^{+0.10}_{-0.09}$	1.57 $^{+0.10}_{-0.08}$	> 65	> 52	> 49	< 1.97	< 1.02	< 1.19
NGC 931	60101002002	0760530201	LW	1.88 $^{+0.07}_{-0.08}$	1.75 $^{+0.05}_{-0.05}$	1.86 $^{+0.05}_{-0.05}$	> 260	> 195	> 248	0.73 $^{+0.27}_{-0.23}$	0.56 $^{+0.20}_{-0.18}$	0.78 $^{+0.23}_{-0.21}$
	60101002004	0760530301	LW	1.89 $^{+0.08}_{-0.06}$	1.81 $^{+0.03}_{-0.03}$	1.88 $^{+0.05}_{-0.03}$	> 367	> 259	> 324	0.80 $^{+0.33}_{-0.25}$	0.60 $^{+0.24}_{-0.18}$	0.84 $^{+0.29}_{-0.21}$
Mrk 1044	60401005002	0824080301	SW	2.50 $^{+0.10}_{-0.09}$	2.42 $^{+0.04}_{-0.04}$	2.48 $^{+0.06}_{-0.04}$	> 126	> 123	> 146	1.75 $^{+0.61}_{-0.50}$	1.31 $^{+0.43}_{-0.37}$	1.52 $^{+0.46}_{-0.39}$
	60401005002	0824080501	SW	2.32 $^{+0.08}_{-0.08}$	2.27 $^{+0.05}_{-0.06}$	2.34 $^{+0.04}_{-0.05}$	> 129	> 129	> 144	0.83 $^{+0.62}_{-0.41}$	1.01 $^{+0.46}_{-0.49}$	1.06 $^{+0.63}_{-0.28}$
3C 109	60301011002	0795600101	LW	1.68 $^{+0.12}_{-0.17}$	1.69 $^{+0.18}_{-0.16}$	1.79 $^{+0.18}_{-0.18}$	> 67	> 74	> 85	< 0.32	< 0.55	< 0.40
NGC 1566	80301601002	0800840201	SW	1.84 $^{+0.03}_{-0.05}$	1.77 $^{+0.02}_{-0.02}$	1.85 $^{+0.03}_{-0.02}$	> 610	> 351	> 475	0.74 $^{+0.16}_{-0.15}$	0.60 $^{+0.12}_{-0.11}$	0.79 $^{+0.15}_{-0.13}$
	80401601002	0820530401	SW	1.77 $^{+0.08}_{-0.09}$	1.60 $^{+0.04}_{-0.03}$	1.69 $^{+0.06}_{-0.04}$	> 241	> 158	> 182	0.67 $^{+0.29}_{-0.25}$	0.49 $^{+0.23}_{-0.20}$	0.64 $^{+0.24}_{-0.22}$
	80502606002	0840800401	SW	1.78 $^{+0.04}_{-0.12}$	1.62 $^{+0.04}_{-0.04}$	1.69 $^{+0.04}_{-0.04}$	> 182	> 106	> 117	0.42 $^{+0.36}_{-0.28}$	0.25 $^{+0.27}_{-0.23}$	0.36 $^{+0.30}_{-0.25}$
1H 0419-577	60402006002	0820360101	SW	1.65 $^{+0.14}_{-0.17}$	1.55 $^{+0.05}_{-0.04}$	1.62 $^{+0.05}_{-0.04}$	63 $^{+46}_{-24}$	52 $^{+31}_{-13}$	56 $^{+35}_{-18}$	< 0.55	< 0.35	< 0.53
	60402006004	0820360201	SW	1.55 $^{+0.19}_{-0.13}$	1.50 $^{+0.05}_{-0.05}$	1.57 $^{+0.05}_{-0.05}$	54 $^{+58}_{-19}$	49 $^{+21}_{-14}$	50 $^{+35}_{-14}$	< 0.52	< 0.40	< 0.60
Ark 120	60001044002	0693781501	SW	1.83 $^{+0.08}_{-0.04}$	1.79 $^{+0.06}_{-0.06}$	1.90 $^{+0.06}_{-0.06}$	> 612	> 714	> 881	0.49 $^{+0.27}_{-0.17}$	0.54 $^{+0.22}_{-0.19}$	0.77 $^{+0.26}_{-0.22}$
	60001044004	0721600401	SW	1.98 $^{+0.03}_{-0.03}$	1.90 $^{+0.02}_{-0.02}$	1.97 $^{+0.02}_{-0.02}$	> 346	> 266	> 335	0.69 $^{+0.18}_{-0.18}$	0.50 $^{+0.15}_{-0.17}$	0.69 $^{+0.17}_{-0.15}$
ESO 362-18	60201046002	0790810101	SW	1.48 $^{+0.14}_{-0.12}$	1.33 $^{+0.04}_{-0.05}$	1.40 $^{+0.06}_{-0.05}$	119 $^{+149}_{-45}$	95 $^{+67}_{-28}$	101 $^{+75}_{-31}$	0.56 $^{+0.39}_{-0.31}$	0.42 $^{+0.29}_{-0.24}$	0.57 $^{+0.32}_{-0.27}$
2MASX J05210136-2521450	60201022002	0790580101	FF	2.11 $^{+0.17}_{-0.17}$	2.12 $^{+0.14}_{-0.14}$	2.24 $^{+0.14}_{-0.14}$	> 114	> 103	> 115	< 0.87	< 0.94	0.57 $^{+0.66}_{-0.47}$
Mrk 79	60601010004	0870880101	SW	1.77 $^{+0.16}_{-0.08}$	1.77 $^{+0.05}_{-0.05}$	1.86 $^{+0.11}_{-0.06}$	> 64	121 $^{+575}_{-54}$	> 75	0.62 $^{+0.61}_{-0.42}$	0.61 $^{+0.50}_{-0.40}$	0.80 $^{+0.55}_{-0.43}$
Mrk 110	60502022002	0852590101	SW	1.87 $^{+0.13}_{-0.13}$	1.70 $^{+0.05}_{-0.05}$	1.78 $^{+0.11}_{-0.06}$	> 114	> 77	> 94	< 0.39	< 0.19	< 0.25
	60502022004	0852590201	SW	1.87 $^{+0.11}_{-0.11}$	1.74 $^{+0.08}_{-0.04}$	1.85 $^{+0.08}_{-0.07}$	> 111	> 86	> 93	0.38 $^{+0.37}_{-0.30}$	< 0.52	0.39 $^{+0.32}_{-0.27}$
NGC 2992	90501623002	0840920301	SW	1.67 $^{+0.04}_{-0.04}$	1.56 $^{+0.03}_{-0.03}$	1.67 $^{+0.03}_{-0.03}$	353 $^{+545}_{-134}$	302 $^{+278}_{-99}$	377 $^{+515}_{-138}$	< 0.16	< 0.09	0.13 $^{+0.08}_{-0.07}$
MCG -05-23-016	60701014002	0890670101	SW	1.83 $^{+0.05}_{-0.05}$	1.80 $^{+0.03}_{-0.03}$	1.91 $^{+0.03}_{-0.03}$	110 $^{+29}_{-19}$	109 $^{+24}_{-17}$	124 $^{+32}_{-21}$	0.77 $^{+0.17}_{-0.15}$	0.72 $^{+0.14}_{-0.13}$	0.96 $^{+0.17}_{-0.15}$
NGC 3227	60202002002	0782520201	SW	1.80 $^{+0.10}_{-0.10}$	1.61 $^{+0.06}_{-0.06}$	1.72 $^{+0.06}_{-0.06}$	189 $^{+260}_{-73}$	147 $^{+104}_{-44}$	171 $^{+147}_{-56}$	1.20 $^{+0.40}_{-0.33}$	0.84 $^{+0.27}_{-0.23}$	1.03 $^{+0.30}_{-0.26}$
	60202002004	0782520301	SW	1.61 $^{+0.13}_{-0.11}$	1.52 $^{+0.07}_{-0.07}$	1.64 $^{+0.07}_{-0.07}$	98 $^{+64}_{-29}$	104 $^{+57}_{-28}$	115 $^{+69}_{-33}$	0.88 $^{+0.41}_{-0.33}$	0.83 $^{+0.33}_{-0.27}$	1.02 $^{+0.36}_{-0.30}$
	60202002006	0782520401	SW	1.82 $^{+0.08}_{-0.08}$	1.62 $^{+0.06}_{-0.05}$	1.73 $^{+0.06}_{-0.06}$	> 166	186 $^{+192}_{-65}$	219 $^{+290}_{-83}$	0.94 $^{+0.32}_{-0.27}$	0.66 $^{+0.23}_{-0.20}$	0.83 $^{+0.26}_{-0.22}$
	60202002008	0782520501	SW	1.86 $^{+0.05}_{-0.07}$	1.69 $^{+0.05}_{-0.04}$	1.80 $^{+0.05}_{-0.05}$	> 510	> 262	> 330	0.89 $^{+0.25}_{-0.23}$	0.63 $^{+0.19}_{-0.17}$	0.79 $^{+0.21}_{-0.19}$
	60202002010	0782520601	SW	1.81 $^{+0.07}_{-0.06}$	1.70 $^{+0.04}_{-0.03}$	1.81 $^{+0.04}_{-0.04}$	244 $^{+312}_{-89}$	207 $^{+156}_{-64}$	255 $^{+256}_{-88}$	0.94 $^{+0.26}_{-0.23}$	0.79 $^{+0.20}_{-0.17}$	0.99 $^{+0.22}_{-0.20}$
	60202002012	0782520701	SW	1.92 $^{+0.07}_{-0.08}$	1.77 $^{+0.05}_{-0.05}$	1.88 $^{+0.05}_{-0.05}$	> 322	> 234	> 295	1.06 $^{+0.33}_{-0.28}$	0.79 $^{+0.23}_{-0.21}$	0.98 $^{+0.26}_{-0.23}$
	80502609002	0844341301	SW	1.60 $^{+0.10}_{-0.10}$	1.68 $^{+0.07}_{-0.07}$	1.79 $^{+0.07}_{-0.07}$	167 $^{+319}_{-69}$	> 132	> 149	0.33 $^{+0.25}_{-0.21}$	0.48 $^{+0.24}_{-0.21}$	0.65 $^{+0.27}_{-0.23}$
	80502609004	0844341401	SW	1.61 $^{+0.23}_{-0.23}$	1.35 $^{+0.15}_{-0.14}$	1.46 $^{+0.15}_{-0.14}$	> 68	84 $^{+142}_{-34}$	90 $^{+161}_{-37}$	0.68 $^{+0.77}_{-0.51}$	0.45 $^{+0.54}_{-0.39}$	0.61 $^{+0.61}_{-0.43}$
2MASSi J1031543-141651	60701046002	0890410101	SW	1.79 $^{+0.13}_{-0.07}$	1.75 $^{+0.04}_{-0.04}$	1.82 $^{+0.07}_{-0.04}$	153 $^{+412}_{-62}$	143 $^{+229}_{-54}$	169 $^{+340}_{-70}$	0.70 $^{+0.41}_{-0.33}$	0.55 $^{+0.31}_{-0.26}$	0.74 $^{+0.35}_{-0.29}$
NGC 3516	60160001002	0854591101	SW	1.70 $^{+0.19}_{-0.15}$	1.69 $^{+0.11}_{-0.11}$	1.80 $^{+0.11}_{-0.11}$	> 90	> 106	> 117	0.77 $^{+0.69}_{-0.50}$	0.86 $^{+0.58}_{-0.44}$	1.09 $^{+0.66}_{-0.50}$
HE 1136-2304	80002031002	0741260101	SW	1.78 $^{+0.16}_{-0.16}$	1.65 $^{+0.11}_{-0.11}$	1.76 $^{+0.11}_{-0.11}$	> 85	> 78	> 84	< 0.79	< 0.54	< 0.72
	80002031003	0741260101	SW	1.60 $^{+0.09}_{-0.09}$	1.51 $^{+0.06}_{-0.06}$	1.58 $^{+0.06}_{-0.06}$	110 $^{+376}_{-55}$	85 $^{+91}_{-35}$	100 $^{+269}_{-47}$	< 0.50	< 0.34	< 0.48
KUG 1141+371	90601618002	0871190101	SW	1.79 $^{+0.33}_{-0.23}$	1.70 $^{+0.08}_{-0.08}$	1.77 $^{+0.13}_{-0.08}$	40 $^{+102}_{-17}$	39 $^{+67}_{-14}$	43 $^{+71}_{-16}$	0.94 $^{+1.50}_{-0.88}$	< 1.39	< 1.59
2MASX J11454045-1827149	60302002002	0795580101	SW	1.74 $^{+0.15}_{-0.14}$	1.63 $^{+0.10}_{-0.05}$	1.74 $^{+0.10}_{-0.08}$	64 $^{+62}_{-22}$	58 $^{+44}_{-18}$	61 $^{+49}_{-19}$	0.51 $^{+0.51}_{-0.39}$	0.32 $^{+0.38}_{-0.31}$	0.46 $^{+0.42}_{-0.34}$
	60302002004	0795580201	SW	1.67 $^{+0.18}_{-0.09}$	1.54 $^{+0.06}_{-0.06}$	1.61 $^{+0.06}_{-0.06}$	> 54	95 $^{+253}_{-42}$	111 $^{+367}_{-53}$	< 0.84	< 0.34	< 0.45
	60302002006	0795580301	SW	1.75 $^{+0.16}_{-0.08}$	1.70 $^{+0.04}_{-0.04}$	1.77 $^{+0.04}_{-0.04}$	126 $^{+593}_{-53}$	121 $^{+239}_{-48}$	138 $^{+357}_{-58}$	< 0.64	< 0.41	0.26 $^{+0.30}_{-0.25}$
	60302002008	0795580401	SW	1.89 $^{+0.14}_{-0.15}$	1.72 $^{+0.04}_{-0.04}$	1.82 $^{+0.10}_{-0.07}$	> 91	> 69	> 74	0.43 $^{+0.50}_{-0.39}$	< 0.64	0.41 $^{+0.42}_{-0.34}$
	60302002010	0795580501	SW	1.90 $^{+0.19}_{-0.19}$	1.73 $^{+0.05}_{-0.05}$	1.79 $^{+0.10}_{-0.03}$	> 78	> 67	> 69	0.50 $^{+0.56}_{-0.49}$	< 0.54	< 0.75
NGC 4051	60401009002	0830430201	SW	1.97 $^{+0.09}_{-0.09}$	1.86 $^{+0.05}_{-0.04}$	1.94 $^{+0.07}_{-0.04}$	> 791	> 446	> 588	1.67 $^{+0.60}_{-0.48}$	1.36 $^{+0.48}_{-0.39}$	1.61 $^{+0.53}_{-0.41}$
NGC 4593	60001149002	0740920201	SW	1.87 $^{+0.18}_{-0.13}$	1.75 $^{+0.10}_{-0.06}$	1.82 $^{+0.13}_{-0.06}$	> 132	> 105	> 115	0.88 $^{+0.92}_{-0.54}$	0.64 $^{+0.67}_{-0.44}$	0.83 $^{+0.75}_{-0.47}$
	60001149004	0740920301	SW	1.73 $^{+0.25}_{-0.20}$	1.53 $^{+0.23}_{-0.05}$	1.64 $^{+0.23}_{-0.14}$	> 142	> 119	> 129	< 1.42	< 1.07	< 1.30
	60001149006	0740920401	SW	1.79 $^{+0.12}_{-0.11}$	1.62 $^{+0.06}_{-0.06}$	1.69 $^{+0.06}_{-0.06}$	> 204	> 98	> 11			

Table 1 (*continued*)

Source	Nu ID	XMM ID	Mode	Γ^{Nu}	Γ^{pn}	$\Gamma^{\text{pn-Cor}}$	$E_{\text{cut}}^{\text{Nu}}$	$E_{\text{cut}}^{\text{Joint}}$	$E_{\text{cut}}^{\text{Joint-Cor}}$	R^{Nu}	R^{Joint}	$R^{\text{Joint-Cor}}$
				keV	keV	keV						
IC 4329A	60001047003	0693781301	SW	$2.24^{+0.05}_{-0.05}$	$2.10^{+0.04}_{-0.04}$	$2.21^{+0.04}_{-0.04}$	> 693	> 318	> 503	$1.75^{+0.35}_{-0.31}$	$1.41^{+0.26}_{-0.23}$	$1.80^{+0.32}_{-0.26}$
	60001047005	0693781401	SW	$2.12^{+0.11}_{-0.12}$	$2.07^{+0.10}_{-0.09}$	$2.18^{+0.10}_{-0.09}$	> 281	> 326	> 425	$1.87^{+0.88}_{-0.66}$	$1.74^{+0.69}_{-0.53}$	$2.06^{+0.78}_{-0.60}$
	60702050002	0862090101	SW	$1.82^{+0.10}_{-0.11}$	$1.75^{+0.07}_{-0.07}$	$1.86^{+0.07}_{-0.07}$	> 138	> 142	> 164	$0.58^{+0.33}_{-0.27}$	$0.51^{+0.26}_{-0.23}$	$0.68^{+0.30}_{-0.25}$
	60702050004	0862090301	SW	$1.74^{+0.11}_{-0.12}$	$1.67^{+0.08}_{-0.08}$	$1.78^{+0.08}_{-0.08}$	> 227	> 204	> 237	< 0.54	< 0.39	$0.28^{+0.27}_{-0.20}$
	60702050006	0862090501	SW	$1.79^{+0.07}_{-0.07}$	$1.74^{+0.06}_{-0.06}$	$1.85^{+0.06}_{-0.06}$	> 450	> 398	> 530	$0.26^{+0.20}_{-0.17}$	$0.21^{+0.16}_{-0.14}$	$0.36^{+0.18}_{-0.16}$
NGC 5548	60702050010	0862090901	SW	$1.79^{+0.34}_{-0.28}$	$1.58^{+0.17}_{-0.10}$	$1.66^{+0.20}_{-0.10}$	> 24	> 24	> 25	< 2.46	< 1.33	< 1.60
	60002044003	0720110601	SW	$1.77^{+0.08}_{-0.08}$	$1.65^{+0.06}_{-0.05}$	$1.76^{+0.06}_{-0.05}$	> 186	> 177	> 214	$0.64^{+0.26}_{-0.22}$	$0.45^{+0.19}_{-0.17}$	$0.61^{+0.21}_{-0.19}$
	60002044005	07201111001	SW	$1.52^{+0.09}_{-0.09}$	$1.53^{+0.06}_{-0.06}$	$1.64^{+0.06}_{-0.06}$	94^{+39}_{-23}	102^{+42}_{-23}	113^{+51}_{-28}	$0.46^{+0.22}_{-0.20}$	$0.52^{+0.21}_{-0.18}$	$0.69^{+0.23}_{-0.20}$
ESO 511-G030	60002044008	0720111501	SW	$1.50^{+0.10}_{-0.11}$	$1.45^{+0.07}_{-0.07}$	$1.56^{+0.07}_{-0.07}$	107^{+68}_{-31}	108^{+55}_{-28}	119^{+67}_{-32}	$0.38^{+0.24}_{-0.21}$	$0.34^{+0.20}_{-0.17}$	$0.46^{+0.21}_{-0.19}$
	60502035002	0852010101	SW	$1.72^{+0.33}_{-0.26}$	$1.56^{+0.17}_{-0.10}$	$1.60^{+0.18}_{-0.10}$	> 40	> 42	> 44	< 1.51	< 0.70	< 0.80
	60502035004	0852010201	SW	$1.73^{+0.24}_{-0.22}$	$1.51^{+0.19}_{-0.10}$	$1.58^{+0.23}_{-0.09}$	> 82	> 54	> 60	< 0.37	< 0.45	< 0.52
	60502035006	0852010301	SW	$1.45^{+0.15}_{-0.17}$	$1.47^{+0.11}_{-0.10}$	$1.54^{+0.10}_{-0.09}$	> 30	52^{+82}_{-21}	66^{+199}_{-30}	< 0.76	< 0.50	< 0.58
Mrk 1383	60502035008	0852010401	SW	$1.57^{+0.16}_{-0.16}$	$1.54^{+0.10}_{-0.10}$	$1.61^{+0.10}_{-0.10}$	> 35	> 34	> 36	< 1.23	< 1.19	< 1.43
	60501049002	0852210101	SW	$1.77^{+0.10}_{-0.10}$	$1.77^{+0.06}_{-0.06}$	$1.84^{+0.06}_{-0.06}$	> 84	> 80	> 89	$0.55^{+0.63}_{-0.42}$	$0.57^{+0.56}_{-0.42}$	$0.78^{+0.63}_{-0.46}$
	60702008002	0882340601	LW	$2.16^{+0.09}_{-0.08}$	$2.15^{+0.07}_{-0.06}$	$2.26^{+0.08}_{-0.06}$	> 988	> 1112	> 1310	$1.57^{+0.54}_{-0.44}$	$1.36^{+0.38}_{-0.33}$	$1.64^{+0.42}_{-0.36}$
Mrk 817	60702008004	0882340701	LW	$1.70^{+0.16}_{-0.16}$	$1.77^{+0.10}_{-0.10}$	$1.88^{+0.10}_{-0.10}$	114^{+244}_{-49}	162^{+704}_{-77}	> 95	$0.95^{+0.60}_{-0.45}$	$0.92^{+0.47}_{-0.38}$	$1.16^{+0.53}_{-0.42}$
	60702008006	0882340801	LW	$1.89^{+0.12}_{-0.18}$	$1.99^{+0.11}_{-0.11}$	$2.10^{+0.11}_{-0.11}$	> 168	> 395	> 497	$1.65^{+0.91}_{-0.42}$	$1.74^{+0.73}_{-0.56}$	$2.05^{+0.81}_{-0.62}$
	60101023002	0763790501	FF	$1.88^{+0.28}_{-0.13}$	$1.94^{+0.15}_{-0.13}$	$2.06^{+0.15}_{-0.14}$	> 62	> 73	> 84	$0.99^{+1.28}_{-0.70}$	$1.02^{+0.93}_{-0.65}$	$1.27^{+1.04}_{-0.71}$
Mrk 841	60702007002	0882130301	SW	$1.85^{+0.14}_{-0.11}$	$1.80^{+0.07}_{-0.04}$	$1.91^{+0.07}_{-0.07}$	> 95	145^{+227}_{-57}	168^{+341}_{-71}	$0.95^{+0.51}_{-0.41}$	$0.90^{+0.40}_{-0.33}$	$1.20^{+0.48}_{-0.38}$
	60702007002	0882130401	SW	$1.90^{+0.10}_{-0.09}$	$1.82^{+0.05}_{-0.04}$	$1.90^{+0.08}_{-0.04}$	> 395	> 295	> 354	$0.66^{+0.39}_{-0.31}$	$0.50^{+0.29}_{-0.23}$	$0.67^{+0.32}_{-0.24}$
	80701616002	0890640201	SW	$1.87^{+0.18}_{-0.13}$	$1.75^{+0.04}_{-0.04}$	$1.84^{+0.09}_{-0.06}$	107^{+264}_{-46}	91^{+121}_{-34}	99^{+147}_{-38}	$1.19^{+0.79}_{-0.57}$	$0.84^{+0.53}_{-0.42}$	$1.10^{+0.61}_{-0.47}$
	60202015002	0790600101	SW	$1.76^{+0.05}_{-0.08}$	$1.72^{+0.10}_{-0.07}$	$1.83^{+0.10}_{-0.10}$	> 140	> 118	> 179	< 0.25	< 0.24	< 0.38
3C 382	60202015004	0790600201	SW	$1.70^{+0.12}_{-0.09}$	$1.61^{+0.08}_{-0.07}$	$1.72^{+0.08}_{-0.08}$	76^{+62}_{-23}	73^{+50}_{-21}	79^{+58}_{-24}	< 0.58	< 0.43	$0.30^{+0.29}_{-0.24}$
	60202015006	0790600301	SW	$1.74^{+0.07}_{-0.06}$	$1.59^{+0.08}_{-0.05}$	$1.68^{+0.07}_{-0.07}$	> 120	144^{+373}_{-63}	> 98	< 0.27	< 0.16	< 0.18
	60202015008	0790600401	SW	$1.76^{+0.15}_{-0.14}$	$1.66^{+0.05}_{-0.04}$	$1.73^{+0.04}_{-0.04}$	> 86	133^{+152}_{-47}	190^{+541}_{-93}	< 0.37	< 0.15	< 0.27
	60202015010	0790600501	SW	$1.77^{+0.05}_{-0.06}$	$1.60^{+0.04}_{-0.04}$	$1.67^{+0.04}_{-0.04}$	> 138	140^{+278}_{-57}	> 97	< 0.26	< 0.11	< 0.14
Fairall 49	60301028002	0795690101	SW	$2.49^{+0.12}_{-0.13}$	$2.33^{+0.08}_{-0.08}$	$2.44^{+0.08}_{-0.08}$	> 116	> 110	> 129	$1.43^{+0.74}_{-0.57}$	$1.05^{+0.52}_{-0.43}$	$1.26^{+0.57}_{-0.46}$
2MASX J19373299-0613046	60101003002	0761870201	SW	$2.42^{+0.16}_{-0.10}$	$2.24^{+0.04}_{-0.03}$	$2.31^{+0.04}_{-0.03}$	> 129	180^{+552}_{-79}	> 115	$1.83^{+0.74}_{-0.61}$	$1.16^{+0.57}_{-0.39}$	$1.31^{+0.56}_{-0.40}$
	60702018004	0891010101	SW	$2.45^{+0.11}_{-0.10}$	$2.33^{+0.07}_{-0.07}$	$2.44^{+0.07}_{-0.07}$	> 220	> 202	> 264	$1.52^{+0.85}_{-0.55}$	$1.32^{+0.80}_{-0.49}$	$1.56^{+0.89}_{-0.52}$
	60702018004	0891010201	SW	$2.30^{+0.09}_{-0.07}$	$2.28^{+0.07}_{-0.06}$	$2.40^{+0.07}_{-0.07}$	> 125	> 120	> 140	$0.78^{+0.36}_{-0.34}$	$1.15^{+0.42}_{-0.37}$	$1.37^{+0.45}_{-0.43}$
NGC 6814	60701012002	0885090101	LW	$1.83^{+0.07}_{-0.07}$	$1.74^{+0.02}_{-0.02}$	$1.80^{+0.04}_{-0.02}$	> 484	> 274	> 353	$0.46^{+0.24}_{-0.20}$	$0.28^{+0.17}_{-0.15}$	$0.46^{+0.19}_{-0.16}$
SWIFT J212745.6+565636	60001110002	0693781701	SW	$1.87^{+0.08}_{-0.05}$	$1.82^{+0.06}_{-0.04}$	$1.93^{+0.06}_{-0.06}$	66^{+20}_{-12}	64^{+20}_{-13}	70^{+24}_{-15}	$1.39^{+0.46}_{-0.35}$	$1.18^{+0.36}_{-0.31}$	$1.50^{+0.43}_{-0.36}$
	60001110003	0693781701	SW	$1.94^{+0.12}_{-0.12}$	$1.89^{+0.07}_{-0.07}$	$2.00^{+0.07}_{-0.07}$	92^{+64}_{-28}	87^{+45}_{-23}	98^{+59}_{-28}	$1.43^{+0.56}_{-0.45}$	$1.36^{+0.44}_{-0.37}$	$1.65^{+0.49}_{-0.41}$
	60001110005	0693781801	SW	$2.00^{+0.07}_{-0.07}$	$1.88^{+0.04}_{-0.04}$	$1.99^{+0.04}_{-0.04}$	87^{+27}_{-17}	73^{+15}_{-11}	82^{+19}_{-13}	$1.73^{+0.36}_{-0.32}$	$1.47^{+0.27}_{-0.24}$	$1.80^{+0.31}_{-0.28}$
	60001110007	0693781901	SW	$1.96^{+0.09}_{-0.08}$	$1.90^{+0.05}_{-0.05}$	$2.01^{+0.05}_{-0.05}$	59^{+16}_{-10}	54^{+11}_{-8}	59^{+14}_{-9}	$1.71^{+0.44}_{-0.38}$	$1.57^{+0.38}_{-0.34}$	$1.92^{+0.42}_{-0.36}$
2MASX J21344509-2725557	60363005002	0802200201	LW	$1.87^{+0.24}_{-0.18}$	$1.77^{+0.19}_{-0.08}$	$1.84^{+0.08}_{-0.08}$	> 46	> 40	> 45	$0.75^{+1.30}_{-0.74}$	< 1.54	$0.80^{+1.20}_{-0.71}$
	60201031002	0790650101	SW	$2.01^{+0.09}_{-0.09}$	$1.93^{+0.06}_{-0.06}$	$2.04^{+0.06}_{-0.06}$	184^{+321}_{-74}	165^{+180}_{-58}	200^{+308}_{-78}	$1.00^{+0.36}_{-0.30}$	$0.90^{+0.32}_{-0.26}$	$1.09^{+0.34}_{-0.28}$
	60002060002	0744490401	LW	$1.75^{+0.09}_{-0.11}$	$1.66^{+0.09}_{-0.09}$	$1.77^{+0.09}_{-0.09}$	> 363	> 290	> 322	< 0.61	< 0.43	$0.32^{+0.31}_{-0.24}$
MR 2251-178	60002060004	0744490501	LW	$1.40^{+0.24}_{-0.23}$	$1.41^{+0.16}_{-0.16}$	$1.52^{+0.16}_{-0.16}$	> 33	74^{+434}_{-36}	> 44	< 0.41	< 0.42	< 0.58
	60002060006	0744490601	LW	$1.75^{+0.48}_{-0.48}$	$1.55^{+0.27}_{-0.23}$	$1.67^{+0.27}_{-0.25}$	> 40	> 39	> 42	< 3.43	< 1.77	< 2.17
	60102025002	0763920501	SW	$1.68^{+0.12}_{-0.10}$	$1.59^{+0.14}_{-0.16}$	$1.70^{+0.12}_{-0.12}$	> 74	> 66	> 75	< 0.10	< 0.08	< 0.10
NGC 7469	60102025004	0763920601	SW	$1.75^{+0.11}_{-0.11}$	$1.63^{+0.07}_{-0.07}$	$1.74^{+0.07}_{-0.07}$	117^{+146}_{-43}	100^{+66}_{-32}	111^{+106}_{-37}	< 0.46	< 0.25	< 0.39
	60102025006	0763920701	SW	$1.86^{+0.11}_{-0.11}$	$1.66^{+0.08}_{-0.08}$	$1.77^{+0.08}_{-0.08}$	> 95	111^{+199}_{-44}	123^{+262}_{-50}	$0.30^{+0.34}_{-0.28}$	< 0.50	$0.25^{+0.30}_{-0.25}$
	60102025008	0763920801	SW	$1.85^{+0.14}_{-0.16}$	$1.63^{+0.08}_{-0.07}$	$1.74^{+0.08}_{-0.08}$	> 78	114^{+132}_{-47}	130^{+412}_{-56}	$0.32^{+0.37}_{-0.31}$	< 0.28	< 0.42
	90601637002	0872390801	SW	$1.58^{+0.14}_{-0.13}$	$1.56^{+0.11}_{-0.11}$	$1.68^{+0.11}_{-0.11}$	67^{+66}_{-23}	74^{+78}_{-26}	79^{+90}_{-28}	< 0.51	< 0.43	< 0.58
	60101001002	0760350201	SW	$1.92^{+0.12}_{-0.07}$	$1.83^{+0.03}_{-0.03}$	$1.91^{+0.07}_{-0.04}$	> 125	> 109	> 125	$0.67^{+0.3$		

Table 1 (*continued*)

Source	Nu ID	XMM ID	Mode	Γ^{Nu}	Γ^{pn}	$\Gamma^{\text{pn-Cor}}$	$E_{\text{cut}}^{\text{Nu}}$	$E_{\text{cut}}^{\text{joint}}$	$E_{\text{cut}}^{\text{joint-Cor}}$	R^{Nu}	R^{joint}	$R^{\text{joint-Cor}}$
				keV	keV	keV						
Mrk 926	60201029002	0790640101	SW	$1.78^{+0.06}_{-0.06}$	$1.70^{+0.05}_{-0.05}$	$1.77^{+0.05}_{-0.05}$	> 184	> 159	> 189	< 0.36	< 0.18	< 0.29
LCRS B232242.2-384320	80502607002	0840800501	SW	$1.75^{+0.10}_{-0.09}$	$1.71^{+0.07}_{-0.07}$	$1.78^{+0.07}_{-0.07}$	> 155	> 155	> 169	< 0.71	< 0.49	$0.28^{+0.42}_{-0.26}$
RX J1231.6+7044	60701055002	0891804001	SW	$1.79^{+0.14}_{-0.11}$	$1.69^{+0.09}_{-0.08}$	$1.75^{+0.11}_{-0.08}$	> 122	> 91	> 133	< 0.29	< 0.15	< 0.19
NGC 4579	60201051002	0790840201	FF	$1.83^{+0.18}_{-0.16}$	$1.92^{+0.17}_{-0.14}$	$1.99^{+0.16}_{-0.13}$	> 60	> 56	> 58	< 0.99	< 1.31	< 1.70
MCG +00-58-028	60001147002	0743010501	FF	$2.00^{+0.27}_{-0.20}$	$1.66^{+0.10}_{-0.10}$	$1.74^{+0.10}_{-0.10}$	> 97	> 29	> 33	$1.15^{+2.27}_{-0.99}$	< 1.23	< 1.46

NOTE— See §3 for the definition of these parameters.

Table 2. Fitting results using *NuSTAR* data alone (without requiring simultaneity with joint XMM exposures)

Source	Nu ID	XMM ID	Nu exp	Overlap Nu exp	Γ	E_{cut}	R
					ks		
Fairall 9	60001130002	0741330101	49.2	3.0	$1.87^{+0.04}_{-0.04}$	> 156	< 1.05
Mrk 359	60402021004	0830550901	49.7	23.6	$1.82^{+0.10}_{-0.09}$	> 109	$0.85^{+0.97}_{-0.58}$
	60402021006	0830551001	51.0	26.9	$1.81^{+0.14}_{-0.07}$	> 205	$0.53^{+0.72}_{-0.43}$
	60402021008	0830551101	48.0	29.1	$1.92^{+0.19}_{-0.20}$	> 85	< 1.97
NGC 931	60101002002	0760530201	63.0	44.6	$1.88^{+0.07}_{-0.07}$	> 253	$0.73^{+0.27}_{-0.23}$
	60101002004	0760530301	64.2	38.7	$1.88^{+0.05}_{-0.06}$	> 343	$0.80^{+0.33}_{-0.25}$
Mrk 1044	60401005002	0824080301	267.1	65.6	$2.49^{+0.05}_{-0.05}$	> 301	$1.75^{+0.61}_{-0.50}$
3C 109	60301011002	0795600101	67.7	28.1	$1.73^{+0.20}_{-0.17}$	> 83	< 0.60
NGC 1566	80301601002	0800840201	56.8	46.4	$1.83^{+0.05}_{-0.05}$	> 453	$0.74^{+0.16}_{-0.15}$
	80401601002	0820530401	75.4	52.7	$1.78^{+0.07}_{-0.07}$	> 352	$0.67^{+0.29}_{-0.25}$
	80502606002	0840800401	57.3	44.7	$1.75^{+0.09}_{-0.14}$	> 190	$0.42^{+0.36}_{-0.28}$
1H 0419-577	60402006002	0820360101	64.2	31.1	$1.67^{+0.13}_{-0.13}$	76^{+55}_{-23}	< 0.55
	60402006004	0820360201	48.3	20.7	$1.59^{+0.11}_{-0.06}$	76^{+34}_{-21}	< 0.52
Ark 120	60001044002	0693781501	55.3	42.5	$1.82^{+0.07}_{-0.04}$	> 557	$0.49^{+0.27}_{-0.17}$
	60001044004	0721600401	65.5	52.0	$1.97^{+0.03}_{-0.03}$	> 588	$0.69^{+0.18}_{-0.18}$
ESO 362-18	60201046002	0790810101	101.9	58.2	$1.55^{+0.09}_{-0.08}$	130^{+97}_{-40}	$0.56^{+0.39}_{-0.31}$
2MASX J05210136-2521450	60201022002	0790580101	155.1	37.0	$2.13^{+0.10}_{-0.09}$	> 218	< 0.87
Mrk 79	60601010004	0870880101	38.5	13.5	$1.80^{+0.05}_{-0.05}$	201^{+523}_{-86}	$0.62^{+0.61}_{-0.42}$
Mrk 110	60502022002	0852590101	86.8	10.8	$1.80^{+0.06}_{-0.06}$	188^{+246}_{-69}	< 0.39
	60502022004	0852590201	88.7	24.5	$1.78^{+0.06}_{-0.06}$	> 166	$0.38^{+0.37}_{-0.30}$
NGC 2992	90501623002	0840920301	57.5	53.1	$1.67^{+0.04}_{-0.04}$	351^{+476}_{-129}	< 0.16
MCG -05-23-016	60701014002	0890670101	83.7	37.7	$1.85^{+0.03}_{-0.03}$	118^{+20}_{-15}	$0.77^{+0.17}_{-0.15}$
NGC 3227	60202002002	0782520201	49.8	25.7	$1.73^{+0.07}_{-0.07}$	165^{+97}_{-46}	$1.20^{+0.40}_{-0.33}$
	60202002004	0782520301	42.5	23.4	$1.61^{+0.09}_{-0.04}$	113^{+58}_{-29}	$0.88^{+0.41}_{-0.33}$
	60202002006	0782520401	39.7	30.3	$1.83^{+0.08}_{-0.08}$	> 206	$0.94^{+0.32}_{-0.27}$
	60202002008	0782520501	41.8	32.7	$1.89^{+0.04}_{-0.03}$	> 652	$0.89^{+0.25}_{-0.23}$
	60202002010	0782520601	40.9	39.1	$1.80^{+0.07}_{-0.05}$	232^{+257}_{-80}	$0.94^{+0.26}_{-0.23}$
2MASSi J1031543-141651	60202002012	0782520701	39.3	29.5	$1.92^{+0.03}_{-0.07}$	> 347	$1.06^{+0.33}_{-0.28}$
	80502609002	0844341301	28.8	25.7	$1.67^{+0.10}_{-0.10}$	> 131	$0.33^{+0.25}_{-0.21}$
	80502609004	0844341401	27.7	20.4	$1.50^{+0.19}_{-0.19}$	> 67	$0.68^{+0.77}_{-0.51}$
	60701046002	0890410101	226.9	47.9	$1.80^{+0.04}_{-0.03}$	159^{+63}_{-39}	$0.70^{+0.41}_{-0.33}$
	60160001002	0854591101	39.9	7.8	$1.96^{+0.06}_{-0.07}$	> 656	$0.77^{+0.69}_{-0.50}$
HE 1136-2304	80002031002	0741260101	23.8	23.7	$1.79^{+0.14}_{-0.16}$	> 92	< 0.79
	80002031003	0741260101	63.6	23.0	$1.60^{+0.05}_{-0.05}$	92^{+78}_{-29}	< 0.50
KUG 1141+371	90601618002	0871190101	38.6	9.7	$1.82^{+0.14}_{-0.09}$	> 73	$0.94^{+1.50}_{-0.88}$
2MASX J11454045-1827149	60302002002	0795580101	21.0	16.7	$1.77^{+0.13}_{-0.13}$	85^{+105}_{-31}	$0.51^{+0.51}_{-0.39}$
	60302002004	0795580201	20.8	12.0	$1.73^{+0.14}_{-0.11}$	> 72	< 0.84

Table 2 *continued*

Table 2 (*continued*)

Source	Nu ID	XMM ID	Nu exp	Overlap	Nu exp	Γ	E_{cut}	R	ks	ks	keV
NGC 4051	60302002006	0795580301	23.1	15.1	$1.75^{+0.06}_{-0.06}$	91^{+60}_{-26}	< 0.64				
	60302002008	0795580401	20.7	14.3	$1.77^{+0.15}_{-0.10}$	122^{+282}_{-52}	$0.43^{+0.50}_{-0.39}$				
	60302002010	0795580501	22.4	13.8	$1.79^{+0.13}_{-0.11}$	> 79	$0.50^{+0.56}_{-0.49}$				
NGC 4593	60401009002	0830430201	311.1	31.5	$2.04^{+0.03}_{-0.03}$	> 2384	$1.67^{+0.60}_{-0.48}$				
MCG -06-30-015	60001149002	0740920201	23.3	8.1	$1.86^{+0.09}_{-0.08}$	> 269	$0.88^{+0.92}_{-0.54}$				
	60001149004	0740920301	21.7	4.6	$1.78^{+0.11}_{-0.11}$	> 543	< 1.42				
	60001149006	0740920401	21.3	11.2	$1.72^{+0.07}_{-0.07}$	> 292	$1.18^{+0.89}_{-0.56}$				
IC 4329A	60001149008	0740920501	23.1	8.0	$1.82^{+0.05}_{-0.05}$	> 1291	$0.67^{+0.49}_{-0.35}$				
	60001149010	0740920601	21.2	12.3	$1.83^{+0.09}_{-0.08}$	> 186	$0.40^{+0.46}_{-0.31}$				
	60001047003	0693781301	127.2	64.1	$2.27^{+0.02}_{-0.04}$	> 736	$1.75^{+0.35}_{-0.31}$				
NGC 5548	60001047005	0693781401	29.6	15.1	$2.15^{+0.04}_{-0.11}$	> 295	$1.87^{+0.88}_{-0.66}$				
	60702050002	0862090101	20.6	6.7	$1.77^{+0.06}_{-0.06}$	> 201	$0.58^{+0.33}_{-0.27}$				
	60702050004	0862090301	20.1	6.2	$1.70^{+0.07}_{-0.07}$	> 206	< 0.54				
ESO 511-G030	60702050006	0862090501	19.8	11.0	$1.83^{+0.02}_{-0.07}$	> 404	$0.26^{+0.20}_{-0.17}$				
	60702050010	0862090901	18.0	1.2	$1.78^{+0.07}_{-0.07}$	> 171	< 2.46				
	60002044003	0720110601	27.3	27.2	$1.77^{+0.08}_{-0.08}$	> 192	$0.64^{+0.26}_{-0.22}$				
Mrk 1383	60002044005	0720111001	49.5	28.7	$1.55^{+0.03}_{-0.08}$	86^{+20}_{-17}	$0.46^{+0.22}_{-0.20}$				
	60002044008	0720111501	50.1	24.5	$1.49^{+0.07}_{-0.07}$	89^{+26}_{-17}	$0.38^{+0.24}_{-0.21}$				
	60502035002	0852010101	32.1	16.5	$1.70^{+0.09}_{-0.26}$	> 40	< 1.51				
Mrk 817	60502035004	0852010201	34.1	18.0	$1.71^{+0.20}_{-0.27}$	> 48	< 0.37				
	60502035006	0852010301	31.2	17.4	$1.56^{+0.14}_{-0.11}$	> 57	< 0.29				
	60502035008	0852010401	41.8	19.8	$1.64^{+0.09}_{-0.10}$	> 76	< 1.23				
Mrk 841	60501049002	0852210101	96.0	38.0	$1.88^{+0.07}_{-0.07}$	> 142	$0.55^{+0.63}_{-0.42}$				
	60702008002	0882340601	65.0	57.8	$2.16^{+0.06}_{-0.08}$	> 1150	$1.57^{+0.54}_{-0.44}$				
	60702008004	0882340701	71.7	52.4	$1.74^{+0.14}_{-0.14}$	120^{+176}_{-47}	$0.95^{+0.60}_{-0.45}$				
3C 382	60702008006	0882340801	78.0	52.1	$1.95^{+0.09}_{-0.16}$	> 267	$1.65^{+0.91}_{-0.42}$				
	60101023002	0763790501	23.4	8.9	$1.83^{+0.12}_{-0.10}$	> 127	$0.99^{+1.28}_{-0.70}$				
	60702007002	0882130301	179.6	59.5	$1.87^{+0.07}_{-0.07}$	275^{+577}_{-116}	$0.95^{+0.51}_{-0.41}$				
Fairall 49	80701616002	0890640201	53.1	28.0	$1.95^{+0.11}_{-0.12}$	> 158	$1.19^{+0.79}_{-0.57}$				
	60202015002	0790600101	23.1	9.5	$1.75^{+0.07}_{-0.08}$	> 133	< 0.63				
	60202015004	0790600201	24.6	12.2	$1.70^{+0.04}_{-0.04}$	115^{+67}_{-31}	< 0.58				
SWIFT J212745.6+565636	60202015006	0790600301	20.8	9.0	$1.74^{+0.04}_{-0.04}$	350^{+455}_{-196}	< 0.27				
	60202015008	0790600401	21.7	10.6	$1.69^{+0.10}_{-0.07}$	168^{+489}_{-73}	< 0.37				
	60202015010	0790600501	21.1	8.3	$1.77^{+0.03}_{-0.04}$	> 253	< 0.26				
2MASX J19373299-0613046	60301028002	0795690101	97.8	27.2	$2.42^{+0.07}_{-0.07}$	182^{+442}_{-78}	$1.43^{+0.74}_{-0.57}$				
	60101003002	0761870201	65.5	64.0	$2.41^{+0.10}_{-0.10}$	> 118	$1.83^{+0.74}_{-0.61}$				
	60702018004	0891010201	150.0	55.1	$2.38^{+0.06}_{-0.06}$	> 224	$0.78^{+0.43}_{-0.34}$				
NGC 6814	60701012002	0885090101	128.2	42.0	$1.83^{+0.03}_{-0.04}$	> 644	$0.46^{+0.24}_{-0.20}$				
	60001110002	0693781701	49.2	46.6	$1.88^{+0.08}_{-0.06}$	61^{+15}_{-10}	$1.39^{+0.46}_{-0.35}$				
	60001110003	0693781701	28.8	26.5	$1.96^{+0.12}_{-0.12}$	94^{+63}_{-28}	$1.43^{+0.56}_{-0.45}$				
2MASX J21344509-2725557	60001110005	0693781801	74.6	67.0	$2.00^{+0.07}_{-0.07}$	87^{+25}_{-16}	$1.73^{+0.36}_{-0.32}$				
	60001110007	0693781901	42.1	38.4	$1.96^{+0.08}_{-0.09}$	59^{+19}_{-9}	$1.71^{+0.44}_{-0.38}$				
	60363005002	0802200201	21.1	12.3	$1.74^{+0.28}_{-0.13}$	> 45	$0.75^{+1.30}_{-0.74}$				
NGC 7314	60201031002	0790650101	100.4	30.1	$2.05^{+0.05}_{-0.05}$	345^{+580}_{-138}	$1.00^{+0.36}_{-0.30}$				
	60002060002	0744490401	53.0	36.9	$1.80^{+0.12}_{-0.09}$	> 365	< 0.61				
	60002060004	0744490501	54.2	18.1	$1.54^{+0.13}_{-0.13}$	> 69	< 0.62				
MR 2251-178	60002060006	0744490601	50.7	7.8	$1.62^{+0.19}_{-0.20}$	> 65	< 3.43				
	60102025002	0763920501	23.1	5.6	$1.67^{+0.06}_{-0.07}$	137^{+148}_{-53}	< 0.10				
	60102025004	0763920601	23.2	12.7	$1.75^{+0.07}_{-0.07}$	175^{+263}_{-66}	< 0.46				
60102025006	0763920701	20.6	10.6	$1.82^{+0.08}_{-0.08}$	128^{+118}_{-43}	$0.30^{+0.34}_{-0.28}$					
	60102025008	0763920801	21.7	10.2	$1.79^{+0.10}_{-0.10}$	171^{+437}_{-71}	$0.32^{+0.37}_{-0.31}$				

Table 2 *continued*

Table 2 (*continued*)

Source	Nu ID	XMM ID	Nu exp	Overlap Nu exp	Γ	E_{cut}	R
			ks	ks		keV	
NGC 7469	90601637002	0872390801	23.6	15.9	$1.63^{+0.11}_{-0.10}$	106^{+174}_{-42}	< 0.51
	60101001002	0760350201	21.6	21.4	$1.92^{+0.13}_{-0.08}$	> 119	$0.67^{+0.39}_{-0.30}$
	60101001004	0760350301	20.0	19.9	$1.86^{+0.09}_{-0.08}$	> 222	$0.48^{+0.36}_{-0.26}$
	60101001006	0760350401	22.5	16.8	$1.88^{+0.06}_{-0.05}$	> 312	$0.72^{+0.42}_{-0.30}$
	60101001010	0760350601	20.9	10.7	$1.84^{+0.05}_{-0.05}$	> 304	$0.32^{+0.40}_{-0.26}$
	60101001012	0760350701	21.0	10.5	$1.84^{+0.05}_{-0.05}$	> 768	$0.96^{+0.55}_{-0.40}$
Mrk 926	60101001014	0760350801	23.4	15.8	$1.83^{+0.05}_{-0.05}$	> 201	$0.43^{+0.35}_{-0.23}$
	60201029002	0790640101	106.2	6.1	$1.72^{+0.02}_{-0.02}$	296^{+196}_{-86}	< 0.36
LCRS B232242.2-384320	80502607002	0840800501	54.8	38.6	$1.74^{+0.08}_{-0.07}$	> 196	< 0.71
RX J1231.6+7044	60701055002	0891804001	136.5	18.2	$1.77^{+0.04}_{-0.06}$	> 229	< 0.29
NGC 4579	60201051002	0790840201	117.8	8.1	$1.81^{+0.04}_{-0.05}$	> 125	< 0.09
MCG +00-58-028	60001147002	0743010501	26.7	8.3	$1.96^{+0.15}_{-0.12}$	> 232	$1.15^{+2.27}_{-0.99}$

NOTE—“Nu exp” refers to the net exposure time of *NuSTAR* FPMA using all available GTI, while “Overlap Nu exp” refers to the remaining net exposure after combining the *NuSTAR* GTI with the EPIC-pn GTI of the joint XMM observation. The fitting results in this table are derived with all the available *NuSTAR* data (“Nu exp”), not requiring simultaneity with corresponding EPIC-pn exposure.

REFERENCES

- Akylas, A., & Georganopoulos, I. 2021, A&A, 655, A60, doi: [10.1051/0004-6361/202141186](https://doi.org/10.1051/0004-6361/202141186)
- Arnaud, K. A. 1996, in Astronomical Society of the Pacific Conference Series, Vol. 101, Astronomical Data Analysis Software and Systems V, ed. G. H. Jacoby & J. Barnes, 17
- Baloković, M., Harrison, F. A., Madejski, G., et al. 2020, ApJ, 905, 41, doi: [10.3847/1538-4357/abc342](https://doi.org/10.3847/1538-4357/abc342)
- Brenneman, L. W., Madejski, G., Fuerst, F., et al. 2014, ApJ, 788, 61, doi: [10.1088/0004-637X/788/1/61](https://doi.org/10.1088/0004-637X/788/1/61)
- Cappi, M., De Marco, B., Ponti, G., et al. 2016, A&A, 592, A27, doi: [10.1051/0004-6361/201628464](https://doi.org/10.1051/0004-6361/201628464)
- Carter, J. A., & Read, A. M. 2007, A&A, 464, 1155, doi: [10.1051/0004-6361:20065882](https://doi.org/10.1051/0004-6361:20065882)
- Chiang, J., Reynolds, C. S., Blaes, O. M., et al. 2000, ApJ, 528, 292, doi: [10.1086/308178](https://doi.org/10.1086/308178)
- Dauser, T., Wilms, J., Reynolds, C. S., & Brenneman, L. W. 2010, MNRAS, 409, 1534, doi: [10.1111/j.1365-2966.2010.17393.x](https://doi.org/10.1111/j.1365-2966.2010.17393.x)
- De Luca, A., & Molendi, S. 2004, A&A, 419, 837, doi: [10.1051/0004-6361:20034421](https://doi.org/10.1051/0004-6361:20034421)
- Fabian, A. C., Lohfink, A., Kara, E., et al. 2015, MNRAS, 451, 4375, doi: [10.1093/mnras/stv1218](https://doi.org/10.1093/mnras/stv1218)
- Feigelson, E. D., & Nelson, P. I. 1985, ApJ, 293, 192, doi: [10.1086/163225](https://doi.org/10.1086/163225)
- García, J., Dauser, T., Lohfink, A., et al. 2014, ApJ, 782, 76, doi: [10.1088/0004-637X/782/2/76](https://doi.org/10.1088/0004-637X/782/2/76)
- Haardt, F., & Maraschi, L. 1991, ApJL, 380, L51, doi: [10.1086/186171](https://doi.org/10.1086/186171)
- . 1993, ApJ, 413, 507, doi: [10.1086/173020](https://doi.org/10.1086/173020)
- Harrison, F. A., Craig, W. W., Christensen, F. E., et al. 2013, The Astrophysical Journal, 770, 103, doi: [10.1088/0004-637x/770/2/103](https://doi.org/10.1088/0004-637x/770/2/103)
- Hinkle, J. T., & Mushotzky, R. 2021, MNRAS, 506, 4960, doi: [10.1093/mnras/stab1976](https://doi.org/10.1093/mnras/stab1976)
- Jansen, F., Lumb, D., Altieri, B., et al. 2001, A&A, 365, L1, doi: [10.1051/0004-6361:20000036](https://doi.org/10.1051/0004-6361:20000036)
- Jiang, J., Abdikamalov, A. B., Bambi, C., & Reynolds, C. S. 2022, MNRAS, 514, 3246, doi: [10.1093/mnras/stac1369](https://doi.org/10.1093/mnras/stac1369)
- Kamraj, N., Harrison, F. A., Baloković, M., Lohfink, A., & Brightman, M. 2018, The Astrophysical Journal, 866, 124, doi: [10.3847/1538-4357/aadd0d](https://doi.org/10.3847/1538-4357/aadd0d)
- Kamraj, N., Brightman, M., Harrison, F. A., et al. 2022, ApJ, 927, 42, doi: [10.3847/1538-4357/ac45f6](https://doi.org/10.3847/1538-4357/ac45f6)
- Kang, J., Wang, J., & Kang, W. 2020, ApJ, 901, 111, doi: [10.3847/1538-4357/abadf5](https://doi.org/10.3847/1538-4357/abadf5)
- Kang, J.-L., & Wang, J.-X. 2022, ApJ, 929, 141, doi: [10.3847/1538-4357/ac5d49](https://doi.org/10.3847/1538-4357/ac5d49)
- . 2023, MNRAS, 519, 3635, doi: [10.1093/mnras/stac3598](https://doi.org/10.1093/mnras/stac3598)
- Kang, J.-L., Wang, J.-X., & Kang, W.-Y. 2021, MNRAS, 502, 80, doi: [10.1093/mnras/stab039](https://doi.org/10.1093/mnras/stab039)
- Kara, E., Zoghbi, A., Marinucci, A., et al. 2015, MNRAS, 446, 737, doi: [10.1093/mnras/stu2136](https://doi.org/10.1093/mnras/stu2136)
- Kuntz, K. D., & Snowden, S. L. 2008, A&A, 478, 575, doi: [10.1051/0004-6361:20077912](https://doi.org/10.1051/0004-6361:20077912)
- Lanzuisi, G., Perna, M., Comastri, A., et al. 2016, A&A, 590, A77, doi: [10.1051/0004-6361/201628325](https://doi.org/10.1051/0004-6361/201628325)

- Lanzuisi, G., Gilli, R., Cappi, M., et al. 2019, ApJL, 875, L20, doi: [10.3847/2041-8213/ab15dc](https://doi.org/10.3847/2041-8213/ab15dc)
- Madsen, K. K., Harrison, F. A., Markwardt, C. B., et al. 2015, ApJS, 220, 8, doi: [10.1088/0067-0049/220/1/8](https://doi.org/10.1088/0067-0049/220/1/8)
- Magdziarz, P., & Zdziarski, A. A. 1995, MNRAS, 273, 837, doi: [10.1093/mnras/273.3.837](https://doi.org/10.1093/mnras/273.3.837)
- Mantovani, G., Nandra, K., & Ponti, G. 2016, MNRAS, 458, 4198, doi: [10.1093/mnras/stw596](https://doi.org/10.1093/mnras/stw596)
- Marchesi, S., Zhao, X., Torres-Albà, N., et al. 2022, ApJ, 935, 114, doi: [10.3847/1538-4357/ac80be](https://doi.org/10.3847/1538-4357/ac80be)
- Marinucci, A., Matt, G., Kara, E., et al. 2014, MNRAS, 440, 2347, doi: [10.1093/mnras/stu404](https://doi.org/10.1093/mnras/stu404)
- Matt, G., Baloković, M., Marinucci, A., et al. 2015, MNRAS, 447, 3029, doi: [10.1093/mnras/stu2653](https://doi.org/10.1093/mnras/stu2653)
- Middei, R., Bianchi, S., Petrucci, P. O., et al. 2019, MNRAS, 483, 4695, doi: [10.1093/mnras/sty3379](https://doi.org/10.1093/mnras/sty3379)
- Molina, M., Malizia, A., Bassani, L., et al. 2019, Monthly Notices of the Royal Astronomical Society, 484, 2735, doi: [10.1093/mnras/stz156](https://doi.org/10.1093/mnras/stz156)
- Nandra, K., O'Neill, P. M., George, I. M., & Reeves, J. N. 2007, MNRAS, 382, 194, doi: [10.1111/j.1365-2966.2007.12331.x](https://doi.org/10.1111/j.1365-2966.2007.12331.x)
- Oh, K., Koss, M., Markwardt, C. B., et al. 2018, ApJS, 235, 4, doi: [10.3847/1538-4365/aaa7fd](https://doi.org/10.3847/1538-4365/aaa7fd)
- Pal, I., & Stalin, C. S. 2023, MNRAS, 518, 2529, doi: [10.1093/mnras/stac3254](https://doi.org/10.1093/mnras/stac3254)
- Pal, I., Stalin, C. S., Parker, M. L., Agrawal, V. K., & Marchesi, S. 2022, MNRAS, 517, 3341, doi: [10.1093/mnras/stac2736](https://doi.org/10.1093/mnras/stac2736)
- Panagiotou, C., & Walter, R. 2019, A&A, 626, A40, doi: [10.1051/0004-6361/201935052](https://doi.org/10.1051/0004-6361/201935052)
- . 2020, A&A, 640, A31, doi: [10.1051/0004-6361/201937390](https://doi.org/10.1051/0004-6361/201937390)
- Parker, M. L., Wilkins, D. R., Fabian, A. C., et al. 2014, MNRAS, 443, 1723, doi: [10.1093/mnras/stu1246](https://doi.org/10.1093/mnras/stu1246)
- Ponti, G., Bianchi, S., Muñoz-Darias, T., et al. 2018, MNRAS, 473, 2304, doi: [10.1093/mnras/stx2425](https://doi.org/10.1093/mnras/stx2425)
- Porquet, D., Done, C., Reeves, J. N., et al. 2019, A&A, 623, A11, doi: [10.1051/0004-6361/201834448](https://doi.org/10.1051/0004-6361/201834448)
- Rani, P., Stalin, C. S., & Goswami, K. D. 2019, Monthly Notices of the Royal Astronomical Society, 484, 5113, doi: [10.1093/mnras/stz275](https://doi.org/10.1093/mnras/stz275)
- Read, A. M., & Ponman, T. J. 2003, A&A, 409, 395, doi: [10.1051/0004-6361:20031099](https://doi.org/10.1051/0004-6361:20031099)
- Risaliti, G., Harrison, F. A., Madsen, K. K., et al. 2013, Nature, 494, 449, doi: [10.1038/nature11938](https://doi.org/10.1038/nature11938)
- Sengupta, D., Marchesi, S., Vignali, C., et al. 2023, A&A, 676, A103, doi: [10.1051/0004-6361/202245646](https://doi.org/10.1051/0004-6361/202245646)
- Shu, X. W., Yaqoob, T., & Wang, J. X. 2010, The Astrophysical Journal Supplement Series, 187, 581, doi: [10.1088/0067-0049/187/2/581](https://doi.org/10.1088/0067-0049/187/2/581)
- Silver, R., Torres-Albà, N., Zhao, X., et al. 2022, ApJ, 940, 148, doi: [10.3847/1538-4357/ac9bf8](https://doi.org/10.3847/1538-4357/ac9bf8)
- Strüder, L., Briel, U., Dennerl, K., et al. 2001, A&A, 365, L18, doi: [10.1051/0004-6361:20000066](https://doi.org/10.1051/0004-6361:20000066)
- Tortosa, A., Bianchi, S., Marinucci, A., Matt, G., & Petrucci, P. O. 2018, A&A, 614, A37, doi: [10.1051/0004-6361/201732382](https://doi.org/10.1051/0004-6361/201732382)
- Tortosa, A., Ricci, C., Tombesi, F., et al. 2021, MNRAS, doi: [10.1093/mnras/stab3152](https://doi.org/10.1093/mnras/stab3152)
- Turner, M. J. L., Abbey, A., Arnaud, M., et al. 2001, A&A, 365, L27, doi: [10.1051/0004-6361:20000087](https://doi.org/10.1051/0004-6361:20000087)
- Wilkins, D. R., & Gallo, L. C. 2015, MNRAS, 449, 129, doi: [10.1093/mnras/stv162](https://doi.org/10.1093/mnras/stv162)
- Wu, Y.-J., Wang, J.-X., Cai, Z.-Y., et al. 2020, Science China Physics, Mechanics, and Astronomy, 63, 129512, doi: [10.1007/s11433-020-1611-7](https://doi.org/10.1007/s11433-020-1611-7)
- Zhang, J.-X., Wang, J.-X., & Zhu, F.-F. 2018, ApJ, 863, 71, doi: [10.3847/1538-4357/aacf92](https://doi.org/10.3847/1538-4357/aacf92)